BRL-MR-3886

(2)

MEMORANDUM REPORT BRL-MR-3886

BRL

DTIC FILE COPY

AD-A231 500

AEROBALLISTIC PERFORMANCE OF THE 25MM M910 TPDS-T RANGE LIMITED TRAINING PROJECTILE

PETER PLOSTINS
ROBERT L. McCOY
BARBARA A. WAGONER

JANUARY 1991

APPROVED FOR PUBLIC RELEASE; DISTRIBUTION UNLIMITED.

U.S. ARMY LABORATORY COMMAND

BALLISTIC RESEARCH LABORATORY
ABERDEEN PROVING GROUND, MARYLAND

91 2 04 149

NOTICES

UNCLASSIFIED

REPORT DOCUMENTATION PAGE

Form Approved OMB No. 0704-0188

1. AGENCY USE ONLY *(Leave blank)*

2. REPORT DATE January 1991

3. REPORT TYPE AND DATES COVERED Final 1 Oct 88 - 1 Oct 90

4. TITLE AND SUBTITLE
AEROBALLISTIC PERFORMANCE OF THE 25MM M910 TPDS-T RANGE LIMITED TRAINING PROJECTILE

5. FUNDING NUMBERS
1L162618AH80 ✓

6. AUTHOR(S)
Peter Plostins
Robert L. McCoy
Barbara A. Wagoner

7. PERFORMING ORGANIZATION NAME(S) AND ADDRESS(ES)
US Army Ballistic Research Laboratory
ATTN: SLCBR-LF
Aberdeen Proving Ground, MD 21005-5066

8. PERFORMING ORGANIZATION REPORT NUMBER

9. SPONSORING/MONITORING AGENCY NAME(S) AND ADDRESS(ES)
US Army Ballistic Research Laboratory
ATTN: SLCBR-DD-T
Aberdeen Proving Ground, MD 21005-5066

10. SPONSORING/MONITORING AGENCY REPORT NUMBER
BRL-~~MR~~-3886

11. SUPPLEMENTARY NOTES

12a. DISTRIBUTION/AVAILABILITY STATEMENT
Approved for public release; distribution unlimited.

12b. DISTRIBUTION CODE

13. ABSTRACT *(Maximum 200 words)*

The U.S. Army has developed a 25mm spin-stabilized, sabot-launched, limited-range training projectile for the Bradley Fighting Vehicle M242 Chain Gun. It is designed to be a ballistic match to the service ammunition and is designated the M910 TPDS-T. The acronym stands for "armor-piercing target-practice - traced." The specified maximum range of the projectile is 8000 meters. During prototype testing at Fort Bliss, Texas, it was determined that the maximum range measured by radar was significantly shorter than had been predicted. Subsequent analysis determined that the projectile had anomalous subsonic aeroballistic performance. Firing tables and range safety data were required to certify the projectile for general use; therefore, extensive aeroballistic tests were ordered to determine the supersonic and subsonic aerodynamic characteristics of the projectile. This report documents the results of those aeroballistic tests.

14. SUBJECT TERMS 25mm training projectile; training ammunition; aeroballistic coefficients; spin-stabilized-sabot-launched-projectile; non-linear aeroballistics; BFV 25mm ammunition; aerodynamic characteristics

15. NUMBER OF PAGES 49

16. PRICE CODE

17. SECURITY CLASSIFICATION OF REPORT	18. SECURITY CLASSIFICATION OF THIS PAGE	19. SECURITY CLASSIFICATION OF ABSTRACT	20. LIMITATION OF ABSTRACT
UNCLASSIFIED	UNCLASSIFIED	UNCLASSIFIED	Same as Report

INTENTIONALLY LEFT BLANK.

TABLE OF CONTENTS

INTENTIONALLY LEFT BLANK.

LIST OF FIGURES

LIST OF FIGURES
(continued)

LIST OF TABLES

INTENTIONALLY LEFT BLANK.

I. INTRODUCTION

The armor-piercing target-practice - traced M910 TPDS-T projectile was developed by the U.S. Army to be a ballistic match to the service ammunition fired from the M242 chain gun mounted on the Bradley Fighting Vehicle. The present service projectile is the armor-piercing discarding-sabot - traced M791 APDS-T, which is a spin-stabilized sabot-launched tungsten alloy penetrator. The M791 is shown in Figure (1). The M910 is similar in design, as can be seen in Figures (2a) and (2b). The requirements for an aeroballistic match are given in Reference (1) and are summarized below.

1.) The time of flight difference between the TPDS-T and the M791 APDS-T will be less than 0.50 second at 2000 metres.

2.) The center of impact of the TPDS-T will not vary from that of the M791 APDS-T by more than one milliradian from 0 to 2000 metres.

3.) The TPDS-T will have a maximum range of 8000 metres, which includes the ricochet safety danger zone.

4.) The TPDS-T will have a visible trace from 100 metres to at least 2000 metres.

5.) The TPDS-T will have a dispersion that does not exceed the dispersion of the service ammunition by more than ten percent.

Requirements 1,2,4 and 5 above have been met by the M910 design. This report will discuss the ability of the projectile to satisfy Requirement 3. The training projectile is significantly lighter than the service projectile and the retardation of the training projectile is high in order to limit the range. It relies on a high-mass flow tracer to reduce the drag and satisfy the ballistic match requirements 1,2 and 4 during the early portion of the trajectory. The low mass and high retardation characteristics of the sub-projectile after tracer burnout were required to restrict the maximum range of the projectile to less than 8000 metres. Due to the steep projectile terminal angle of fall the ricochet fan is assumed to be negligible.

Generally the maximum range trajectory of direct-fire service ammunition is of secondary importance; however, in the case of a training projectile it is one of the primary drivers for the design. In order for the developer to obtain safety certifications and releases, the maximum range of the projectile must be well-defined under all firing conditions. The determination of the maximum range requires aerodynamic data along the entire trajectory. Normally only the drag characteristics are needed and point-mass trajectories are computed. Early in the development of this projectile, anomalies in its long-range performance were noted. As described in Reference (1), during long-range testing at Fort Bliss, Texas, the radar data indicated the projectile was falling short of the maximum range that had been predicted by a point-

mass trajectory analysis. Figure (3), which is taken from Reference (1), clearly shows the Midi radar data deviating from the trajectory prediction. Some preliminary aerodynamic data for the projectile were available and were used to do a six-degrees-of-freedom (6 DOF) trajectory analysis. This analysis indicated that the projectile had a subsonic dynamic instability that caused high drag due to yaw and thus reduced the range. This situation is desirable in a training projectile; however, very little aerodynamic data were available and therefore the nature of the instability could not be defined. Reference (1) recommended that extensive aeroballistic tests be performed to define the nature and effects of the instability. The developers - the U.S. Army Armament, Research, Development and Engineering Center (ARDEC) at Picatinny Arsenal in Dover, New Jersey - concurred with the recommendation because they felt that no safety certification could be obtained without accurately defining the maximum range of the projectile.

The U.S. Army Ballistic Research Laboratory (BRL) was tasked by the Close Combat Armament Center of ARDEC to obtain a complete set of aeroballistic coefficients for the M910 projectile, to determine the nature of the anomalies noted during the Fort Bliss radar test and to define an accurate maximum range trajectory. This information could then be used to generate firing tables and to certify the projectile safe for general use by Bradley Cavalry and Infantry Fighting Vehicle Forces.

II. TEST INSTRUMENTATION AND PROCEDURES

The tests were conducted in the BRL Aerodynamics Range Facility. The facility is a 100-metre long spark shadowgraph facility designed to obtain aerodynamic coefficients from free-flight trajectory data. Specific data on the range set-up may be obtained from Reference (2). There are 27 master spark shadowgraph stations arranged in five groups. The first group has seven master stations and the rest have five master stations each. Fifty M910 projectiles were delivered for testing. The projectiles had the tracer cavity filled with an inert trace material. This was required to maintain the same mass and inertial properties as the traced projectile and to enable the range triggering system to identify the projectile. The range triggering system employs infrared light screens to sense the projectile passage. A reduction in light triggers the system. Bright tracers flood the system with too much light, thus obscuring the passage of the projectile. A microcomputer controls the range timing and triggering. The computer presets a delay for each station based on the expected flight velocity. As the projectile is sensed by the infrared screen, the delay countdown is initiated and on completion triggers the spark source. At that instant the projectile is near the center of the film plane. The projectile image is captured on 29.9 by 35.6 cm (11 by 14 inch) film. The range fiducial system is simultaneously recorded on the film. The film is read on digital tablets and the data are reduced by the methods described in Reference (3).

The 50 M910 projectiles were delivered as manufactured, see Figure (2b). The assembly consists of an aluminum pusher, the sub-projectile and a molded glass-filled nylon 6-6 sabot. One sub-projectile was completely cut out of the sabot/pusher assembly. Physical property measurements were made on this sub-projectile. It was assumed that all of the other sub-

projectiles were geometrically and inertially similar. The physical properties of the sub-projectile are presented in Table (1).

The projectiles were launched for a range of Mach numbers from 0.60 to 4.50. Half of the projectiles were launched at supersonic Mach numbers, nominally 4.5, 3.5, 2.5 and 1.4. The other half were launched between Mach 1.0 and 0.6. Data were obtained on a total of 39 projectiles because 11 of the projectiles were expended solving launch problems.

The projectiles were all launched from a 25 mm gain twist Mann barrel. The exit twist of the barrel is 610 mm/turn. The projectiles were loaded into cartridge cases with appropriate charges to produce mean muzzle velocities ranging from 200 to 1540 m/s (Mach 0.6 to 4.5). At muzzle velocities between 400 and 500 m/s (Mach 1.18 and 1.47) the nylon 6-6 sabot failed to separate. The sabot is designed to utilize the centripetal acceleration forces to fracture and separate the petals. As the projectiles were downloaded, the centripetal acceleration loads decreased and were unable to fracture the sabot. The sabots were weakened by scoring the sabot between the petals and radially between the pusher cup body and fingers, see Figure (4). This method succeeded in weakening the sabot sufficiently to allow separation. However, below approximately 250 m/s (Mach 0.75) the sabot again failed to separate, even with the previously described modifications. It became necessary to cut the sabot completely off of the sub-projectile and reassemble it in order to launch the sub-projectile at velocities below 250 m/s.

When the first projectile was launched with a completely reassembled sabot, another launch problem was identified. The sabot/pusher was designed to impart spin to the sub-projectile through the friction force between the 45-degree cone at the base of the projectile and an identical surface machined into the pusher cup. As the propellant charge was reduced, the set-back loads were insufficient to provide enough friction to spin-up the projectile. It was gyroscopically unstable at launch and began to tumble. A 3.185 mm slit was cut into the base of the projectile through the conical surface, see Figure (5), and a 3.175 mm spring pin was fitted through the pusher cup, thus locking both together when assembled. This solved the projectile spin-up problem. The slit in the projectile base was positioned so that it was always in the projectile wake, thus insuring minimal effects on the flow field over the projectile body.

Because the gun has a constant exit twist, the launch gyroscopic stability factor drops as the muzzle velocity is reduced. At subsonic Mach numbers, the gyroscopic stability factor of this projectile drops to approximately 1.5. As the gyroscopic stability factor asymptotically approaches 1.0, the projectile sensitivity to its launch conditions increases, see Reference (4). This launch sensitivity causes an increase in first maximum yaw. Cutting the sabot apart and reassembling it also reduced the inbore stiffness of the sabot/sub-projectile assembly. Higher linear and angular launch rates resulted. The combination of gyroscopic stability factors less than 1.5 and higher initial rates yielded many higher yaw flights. The advantage of this combination of events was that high-yaw data were required at subsonic Mach numbers to investigate the instability characteristics.

Low-yaw data were also required to define completely the subsonic flight regime. The projectile launch rates would have to be reduced and the gyroscopic stability factor increased to acquire the low-yaw data. The latter was accomplished by re-saboting the projectile, as shown in Figure (6), and launching it from a 20-mm cannon with a twist rate of 254 mm/turn. The sabot was machined out of torlon bar stock and the projectile conical base scored as drawn in Figure (6) to provide a positive spin-up mechanism. Two sub-projectiles were launched in this configuration, resulting in the desired low-yaw flights.

III. ANALYSIS OF THE DATA

The free-flight spark range data were fitted to solutions of the linearized equations of motion and the resulting flight motion parameters were used to infer linearized aerodynamic coefficients, using the methods of Reference (3). Preliminary analysis of the aerodynamic data showed distinct variation of several coefficients with yaw level. Murphy in Reference (3) has shown that aerodynamic coefficients derived from the linearized data reduction can be used to infer the coefficients in a nonlinear force and moment expansion, if sufficient data are available. For the M910 projectile, sufficient data were obtained to permit determination of several nonlinear coefficients.

A more recent data reduction technique, Reference (5), utilizes numerical integration of the 6 DOF differential equations of motion, combined with a maximum likelihood method for fitting the numerical solution to the observed flight motion data. Both data reduction methods were applied to the subsonic and transonic M910 data, and good agreement between the two methods was observed. A more detailed discussion of nonlinear behavior is presented in the various subtopics of this section.

A useful by-product of tests conducted in the BRL spark photography ranges is the high-quality shadowgraph information obtained. Figures (7a), (7b), (7c) and (7d) illustrate the flow fields around the M910 projectile at various supersonic, transonic, and subsonic speeds. Figure (7e) is a shadowgraph of the subsonic flow field about the projectile at a high angle of attack. The exact Mach number, view and angle of attack the projectile has in the shadowgraph are given in the figure. Also provided is the angle of attack the projectile has in the orthogonal, view, which is not shown. The angle α is the vertical angle and the angle β is the horizontal angle. A positive vertical angle indicates a nose-up orientation and a positive horizontal angle is a nose-left orientation.

The round-by-round aerodynamic data obtained are listed in Table (2). The observed flight motion parameters are given in Table (3).

a.) Drag Coefficient

The drag coefficient, C_D, is determined by fitting the time-distance measurements from the range flight. C_D varies with yaw level, and the value determined from an individual flight

reflects both the zero-yaw drag coefficient, C_{D_o}, and the induced drag due to the average yaw level of the flight. The drag coefficient variation is expressed as an even power series in yaw amplitude:

$$C_D = C_{D_o} + C_{D_{\delta^2}}\delta^2 + \ldots \tag{1}$$

where $C_{D_{\delta^2}}$ is the quadratic yaw-drag coefficient and δ^2 is the total angle of attack squared.

Figure (8a) illustrates the variation of the zero-yaw drag coefficient with Mach number for the M910 projectile with tracer off. The quadratic yaw-drag coefficient, shown in Figure (8b), was obtained from least-squares fits of the range values of drag coefficient as functions of Mach number and total angle of attack. The yaw-drag coefficients derived from the fits were used to correct the range values of C_D to the zero-yaw values plotted in Figure (8a).

The trajectory analysis in Section IV of this report requires drag data on the M910 with the tracer functioning. It is not possible to obtain these data in the Aerodynamics Range Facility because of the triggering system. These data will be drawn from two other sources. The first source is Reference (1), which presents Midi Radar data from the Fort Bliss test, and the second source is Reference (6), which presents radar data acquired by the Combat Systems Test Activity (CSTA), Aberdeen Proving Ground, Maryland. Figure (9) summarizes all the drag data. In the plot, the squares are the untraced Aerodynamics Range data, the diamonds are the Midi Radar data (Reference (1)) and the triangles are the CSTA Hawk Radar data from Reference (6). The dashed line is the fit of the untraced drag data. The solid line is the drag curve utilized in the trajectory analysis to follow. In the transonic regime, the solid curve is a mean between the traced and untraced drag data.

b.) Overturning Moment Coefficient

The range values of the overturning moment coefficient, C_{M_α}, were fitted using the appropriate squared-yaw from Reference (3). No dependence of C_{M_α} on yaw level was observed for the M910 projectile at speeds above Mach 2.5. At lower supersonic speeds, negative values of the cubic overturning moment were found from the least-squares fit. The cubic coefficient, C_2, was found to be positive at transonic and subsonic speeds. Figure (10a) is a plot of the variation of the zero-yaw overturning moment coefficient, $C_{M_{\alpha o}}$, with Mach number, and Figure (10b) illustrates the cubic coefficient used to reduce the range values of C_{M_α} to zero-yaw conditions.

c.) Gyroscopic Stability

The gyroscopic stability factor of a projectile is defined in Reference (3) as:

$$S_g = \frac{P^2}{4M} \tag{2}$$

where:

$$P = (\frac{I_x}{I_y})(\frac{pd}{V}) \qquad\qquad M = (\frac{\rho S d^3}{2I_y})C_{M_\alpha}$$

A launch gyroscopic stability factor greater than 1.5 is usually desired, to insure ample stability margin under worst-case conditions, such as cold high-density air. Only the launch value of the gyroscopic stability need be considered for high-velocity, flat-fire munitions, since the axial spin-to-velocity ratio increases along the trajectory.

For the M910 projectile, fired from the service barrel with a muzzle twist rate of 610mm/turn, at standard muzzle velocity of 1540 metres/second, and at ICAO sea-level standard atmospheric conditions, the launch gyroscopic stability factor is 2.0, which insures more than sufficient stability margin under worst-case conditions.

d.) Lift Force Coefficient

The range values of the lift force coefficient, $C_{L\alpha}$, were also analyzed using the methods of Reference (3). The cubic lift force coefficient, a_2, for the M910 projectile was found to have a significant negative value at speeds above Mach 1.5, and a much smaller negative value at subsonic speeds. Figure (11a) shows the variation of the zero-yaw lift coefficient, $C_{L\alpha o}$, with Mach number for the M910, and Figure (11b) illustrates the behavior of the cubic lift coefficient at various flight speeds.

The lift coefficient is determined from the swerve reduction in free-flight range tests, and is not as well determined as the overturning moment coefficient, which is obtained from the yaw reduction. The increased scatter in $C_{L\alpha o}$ exhibited in Figure (11a), relative to that of $C_{M\alpha o}$ plotted in Figure (10a), reflects the fact that swerve is less accurately measured in free-flight range tests than is the yawing motion.

e.) Magnus Moment and Pitch Damping Moment Coefficient

The Magnus moment coefficient, $C_{Mp\alpha}$, and the pitch damping moment coefficient sum $C_{Mq}+C_{M\dot{\alpha}}$, are discussed together, since if either coefficient varies with yaw level, both coefficients exhibit coupling in the data reduction process described in Reference (3). Due to this mutual interaction in the data reduction process, the analysis of the two coefficients must be performed simultaneously, even though the aerodynamic moments are not, in themselves, physically related.

If the dependence of the Magnus moment and the pitch damping moment are cubic in yaw level, the nonlinear variation of the two moment coefficients are of the general form:

$$C_{M_{p\alpha}} = C_{M_{p\alpha_o}} + \hat{C}_2\delta^2 \tag{3}$$

$$C_{M_q} + C_{M_{\dot{\alpha}}} = (C_{M_q} + C_{M_{\dot{\alpha}}})_o + d_2\delta^2 \tag{4}$$

where $C_{M_{p\alpha o}}$ and $(C_{M_q}+C_{M_{\dot{\alpha}}})_o$ are the zero-yaw values of Magnus and pitch damping moment coefficients, respectively, and $\hat{C}_2$ and d_2 are the associated cubic coefficients.

In Reference (3) it is shown that the nonlinear coupling introduced through the least squares fitting process yields the following expressions for range values (R-subscript) of the two coefficients:

$$[C_{M_{p\alpha}}]_R = C_{M_{p\alpha_o}} + \hat{C}_2\delta^2_{e_{TT}} + d_2\delta^2_{e_{TH}} \tag{5}$$

$$[(C_{M_q} + C_{M_{\dot{\alpha}}})]_R = (C_{M_q} + C_{M_{\dot{\alpha}}})_o + \hat{C}_2\delta^2_{e_{HH}} + d_2\delta^2_{e_{HT}} \tag{6}$$

where the above effective squared yaws and the remaining symbols are defined in the List of Symbols at the end of this report and completely discussed in Reference (3).

Preliminary analysis of the M910 data showed no significant pitch damping nonlinearity at supersonic speeds, and the supersonic Magnus and pitch damping moment coefficients were analyzed using only a cubic Magnus moment. The value obtained for $\hat{C}_2$ at supersonic speeds was 120.

At transonic and subsonic speeds, the preliminary analysis indicated the presence of significant cubic coefficients in both the Magnus and pitch damping moment terms. The final analysis was performed using both the coupled quasi-linear technique, (i.e., Equations (5) and (6)), and the 6 DOF methods of Reference (5). Good agreement was observed between the two methods; however the 6 DOF cubic coefficients appeared to be better determined, due to the enhancement of the multiple-round data reduction capability. The 6 DOF cubic coefficients were used to correct the range values of $C_{M_{p\alpha}}$ and $C_{M_q}+C_{M_{\dot{\alpha}}}$ to zero-yaw conditions, at transonic and subsonic speeds.

For Mach numbers below 1.0, several rounds were fired at large yaw, and the nonlinear analysis indicated a bi-cubic Magnus moment behavior at subsonic speeds. Bi-cubic Magnus moment behavior occurs when the quadratic Magnus moment term abruptly changes its value at a given angle of attack. This change is usually due to a significant change in the flow field over the projectile. Figure (12a) shows the variation of the Magnus moment coefficient with effective yaw squared at subsonic speeds. The effective yaw squared is taken from Reference (3) and given in Equation (7).

$$\delta_e^2 = K_F^2 + K_S^2 + \frac{\left(\phi'_F K_F^2 - \phi'_S K_S^2\right)}{\left(\phi'_F - \phi'_S\right)} \tag{7}$$

The data in Figure (12a) are centered around the M_∞ = 0.70 bi-cubic. The other bi-cubic curves, ranging from M_∞ = 0.20 to M_∞ = 1.00 are the estimated values of the bi-cubic subsonic Magnus coefficient used in the trajectory analysis. In Figure (7e) leeside boundary layer separation is evident at the nose of the projectile. The angle of attack shown in the shadowgraph is 15.3 degrees. The angle of attack in the vertical shadowgraph is -2.35 degrees. Thus the horizontal view is very close to the plane of total yaw. The Magnus moment is sensitive to leeside separation and alters its variation with angle of attack subsequent to leeside separation. Range measurement of nonlinear Magnus is discussed in Reference (7). Figures (12b) and (13a) illustrate the zero-yaw variation of the Magnus and pitch damping moment coefficients with Mach number. The cubic coefficient used to reduce the range values of $C_{M_{p\alpha}}$ to zero-yaw conditions at supersonic Mach numbers and one data point derived by the methods of Reference (5) are shown in Figure (12c). The corresponding cubic coefficient used to reduce range values of $C_{M_q}+C_{M_{\dot{\alpha}}}$ to zero-yaw conditions is plotted in Figure (13b). The dashed lines in the plots are the estimated behavior of the coefficients below M_∞ = 0.60.

f.) Epicyclic Damping Rates

The damping rates, λ_F and λ_S, of the fast and slow yaw modes indicate the dynamic stability of a projectile. A negative lambda indicates damping; a positive lambda means that the associated modal arm will grow with increasing distance along the trajectory.

For a projectile whose Magnus or pitch damping moment is nonlinear with yaw level, the damping rates also show a nonlinear dependence on yaw. For the M910 projectile, the fast modal arm was observed to be damped at all speeds tested. The slow modal arm is neutrally damped at high supersonic speeds, and is undamped at lower supersonic and transonic speeds, for small angles of attack. At subsonic speeds, the bi-cubic Magnus moment produces a bi-cubic variation of the slow-arm damping rate with effective angle of attack squared; this variation is shown in Figure (14a) at M_∞ = 0.70. The zero-yaw slow arm damping rate behavior at various flight Mach numbers is illustrated in Figure (14b). Again the dashed curve is the estimated behavior below M_∞ = 0.60.

The effect of the bi-cubic slow-arm damping rate at subsonic speeds is a slow-arm limit cycle yaw of approximately 14 degrees magnitude, at flight Mach numbers below 1.0. The 14-degree limit-cycle yaw increases the drag coefficient by about 77 percent. The trajectory analysis in the subsequent section of this report indicates that the sea-level maximum range trajectory is 42 seconds long and 37 seconds of the trajectory is in the subsonic flight regime. This long flight time at a higher drag significantly reduces the maximum range attained by the projectile.

g.) Spin Damping Moment Coefficient

The spin damping moment coefficient, C_{l_p}, is determined by fitting roll angle versus distance measurements from the range. The variation of the spin damping moment coefficient with Mach number is much weaker than that observed for the drag coefficient. No variation of

C_{lp} with yaw level could be found in the M910 data. Figure (15) illustrates the variation of C_{lp} with Mach number for the M910 projectile.

IV. TRAJECTORY ANALYSIS

The basic purpose of the aeroballistic tests was to gather enough aeroballistic data to be able to compute a trajectory for the M910 projectile. The data described in the preceding section was used to compute a 6 DOF maximum range trajectory. Two maximum range trajectories were computed, one at sea level standard conditions taken from the ICAO Standard Atmosphere and the second at the Fort Bliss test conditions. Fort Bliss is located 1250 metres above sea level and the projectiles were conditioned hot and fired on a hot day. The test muzzle velocity was 1590 m/s, the ambient temperature was 32.2°C and the quadrant elevation was 32.5 degrees. This quadrant elevation results in the maximum range. At sea level the maximum range trajectory launch conditions are a muzzle velocity of 1540 m/s and a quadrant elevation of 30 degrees. Figure (16) is a summary comparing the 6 DOF maximum range trajectories computed at Fort Bliss test conditions with the point-mass trajectory and the Midi Radar data. Clearly, the 6 DOF trajectory is closer to the Midi radar data than the point-mass trajectory. The 6 DOF trajectory still predicts a longer range than the data would indicate. The present prediction results in a conservative estimation of the maximum range.

In Figure (16) the Midi data appears to deviate from the point mass (PTM) prediction at approximately 5000 metres. From Figure (17) it can be inferred that Mach one occurs at approximately 3800 metres. The 6 DOF prediction still under-estimates the drag at transonic and subsonic Mach numbers. This result is clearer in Figure (18), a plot of the predicted variation of velocity with range compared to the Midi radar data. The velocity is overpredicted as the range increases. The basic shape of the 6 DOF trajectory plotted in Figure (16) is more consistent with the Midi radar data trajectory. The majority of the trajectory is subsonic, see Figure (19). For the Fort Bliss conditions, Mach 1.0 occurs at about six seconds and total flight time is 49 seconds. Mach 1.0 occurs at 3800 metres, see Figure (17), and in Figure (20) the projectile total angle of attack begins to increase just prior to Mach 1.0. It continues to increase, reaching a limit cycle of about 14 degrees. Because the angle of attack increase begins at 3800 metres the 6 DOF trajectory actually begins to diverge from the PTM trajectory at the Mach one point, but the deviation is so gradual that it is not obvious in Figure (16).

The trajectory model launched the projectile with approximately one degree initial maximum yaw. The nonlinear Magnus moment and pitch damping moment characteristics displayed by the projectile are also evident in the variation of its dynamic stability factor with range, Figure (21). The dependence of the dynamic stability factor on the projectile aerodynamic coefficients is given in Equation (8).

$$S_d = \frac{2[C_{L_\alpha} + k_x^{-2} C_{M_{p\alpha}}]}{[C_{L_\alpha} - C_D - k_y^{-2}(C_{M_q} + C_{M_{\dot\alpha}})]} \qquad (8)$$

At supersonic Mach numbers the dynamic stability factor, plotted in Figure (21), is between zero and two. As discussed in Reference (3), the dynamic stability factor must remain in this range for the projectile to remain dynamically stable. Just above Mach 1.0 it becomes negative, subsequently exhibiting large oscillations during the transonic and high subsonic regime and finally oscillating about zero during the limit cycle. The projectile can be expected to consistently and repeatedly exhibit these trajectory characteristics and hence have a significantly shorter maximum range.

The 6 DOF trajectory model does basically describe the phenomena that result in the shorter maximum range of the M910. The increased yaw at subsonic Mach numbers is the cause of the lower maximum range. The trajectory model still overpredicts the range when the results are compared to the Midi radar data. It appears that the yaw rise during transonic Mach numbers may occur earlier and faster than the present model predicts. Insufficient data between Mach 1.5 and 0.95 were obtained to determine precisely the aerodynamic behavior in this region. Apparently the limit cycle grows larger at very low subsonic Mach numbers, for instance Mach 0.4 and below, since a lower drag is predicted than required to match the radar data trajectory. It is difficult to acquire very low subsonic data in the Aerodynamics Range Facility because the flight window is too small. At such low velocities the trajectory curvature is very large and the projectile does not remain in the flight window long enough for sufficient data to be collected. The data can be obtained from further testing but the present model provides a good conservative estimate of the maximum range.

The 6 DOF trajectory analysis predicts that the maximum range of the projectile at Fort Bliss conditions is 7680 metres, the terminal velocity is 124.4 m/s and the angle of fall is 83.25 degrees. The actual maximum range is probably 200 to 250 metres lower. At sea level the maximum range predicted is 6128 metres, the terminal velocity is 110 m/s and the angle of fall is 81.97 degrees. A 200 to 250 metre shorter maximum range can also be expected in this case. The sea-level trajectory results are presented in Figures (22) and (23). It should be noted that the projectile is coning in its limit cycle as it impacts so it actually impacts at some point on a cone 14 degrees off of the mean angle of fall given above. This fact needs to be considered in any ricochet analysis.

V. CONCLUSIONS

An extensive aeroballistic data set has been obtained for the M910 limited-range training projectile. Both linear and nonlinear aerodynamic coefficients were determined over a Mach number range of 0.60 to 4.50. The aerodynamic data were used to predict the maximum range trajectories of the projectile at Fort Bliss and sea-level launch conditions. The computed trajectory was found to predict a longer maximum range of the projectile than indicated by the Midi radar data at Fort Bliss conditions; however, the basic trajectory shape is consistent with the observed radar trajectory. The shorter maximum range trajectories were found to be the result of a nonlinear pitch damping moment coefficient and a bi-cubic Magnus moment coefficient at transonic and subsonic Mach numbers. The result of these aerodynamic moments is to produce a

large-yaw limit cycle during a large part of the trajectory, causing higher drag and thus reducing the range.

More data would be required at transonic and low subsonic Mach numbers to define the trajectory precisely and provide a closer prediction of the Fort Bliss Midi radar trajectory. The present data provide the basic aeroballistic characteristics of the projectile but the additional data would help refine the model. This aeroballistic behavior appears to be characteristic of spin-stabilized cone-cylinder projectiles and is beneficial to the design of limited-range training projectiles.

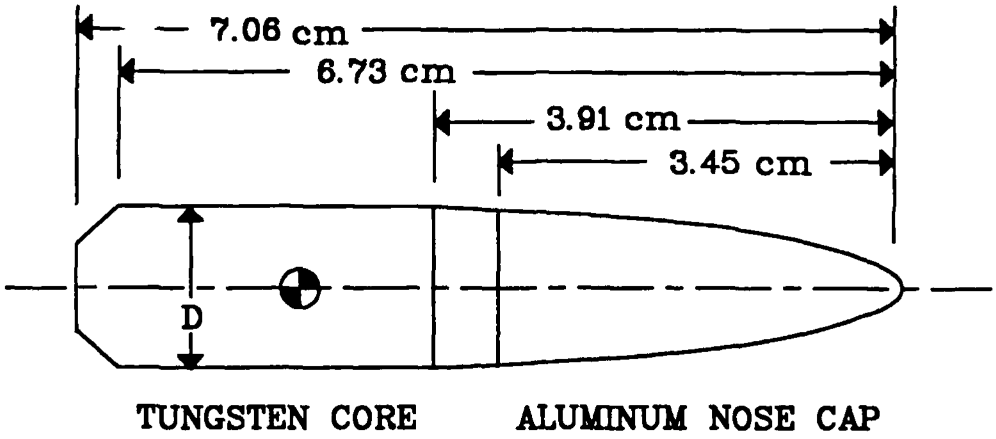

$d = 1.35$ cm
$l/d = 5.24$
$m = 104.5$ gm
$I_x = 21.9$ gm–cm^2
$I_y = 176.0$ gm–cm^2
$V = 1345$ m/s
$X_{c.m.} = 4.70$ cm (from the nose)

Figure (1) Schematic of the M791 APDS-T Service Projectile

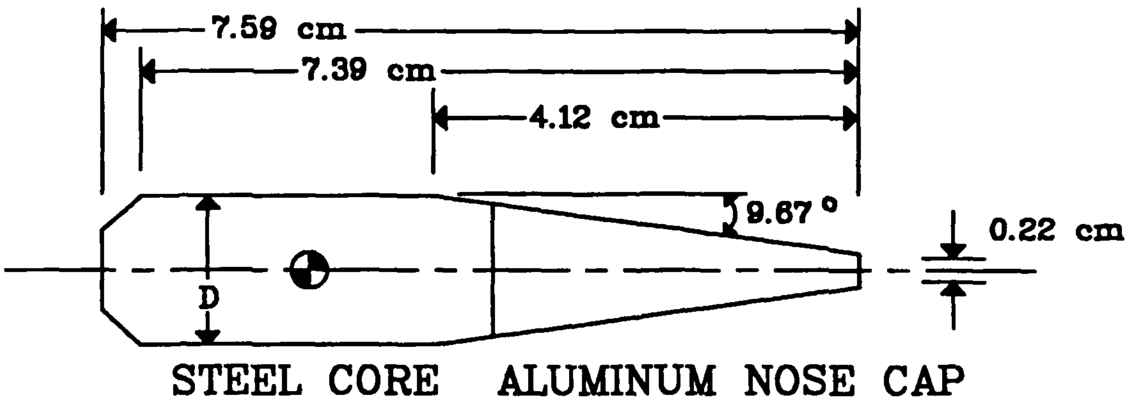

$d = 1.62$ cm
$l/d = 4.69$
$m = 66.9$ gms
$I_x = 21.57$ gm–cm^2
$I_y = 146.87$ gm–cm^2
$V = 1540$ m/s
$X_{c.m.} = 4.47$ cm (from the nose)

Figure (2a) Schematic of the M910 TPDS-T Training Projectile

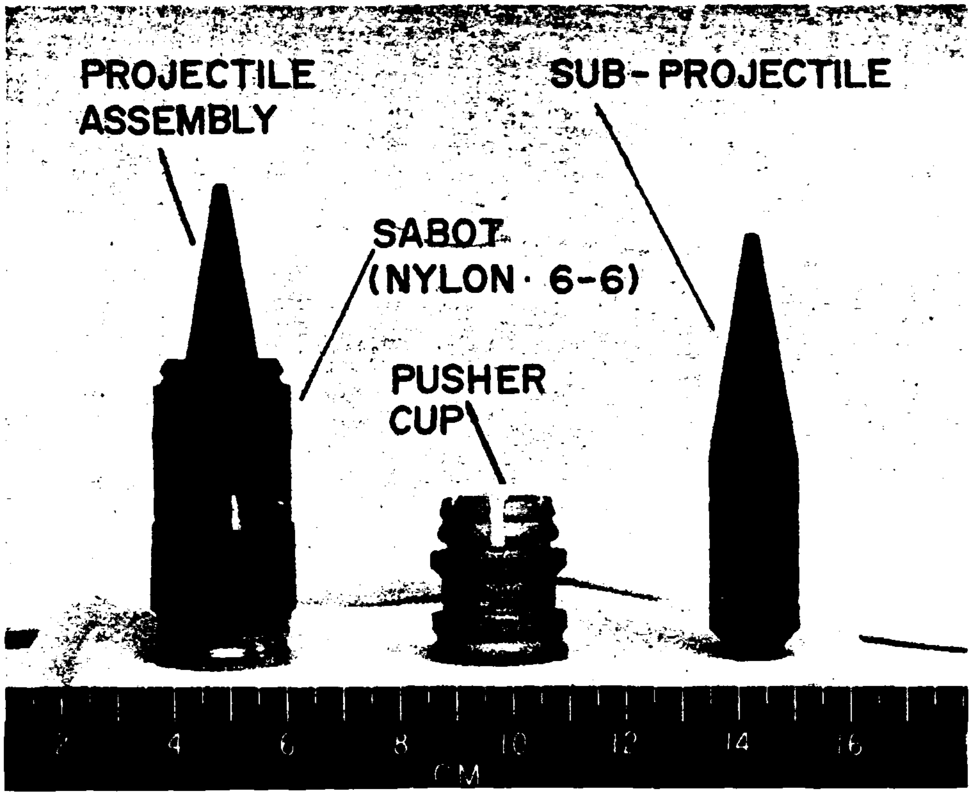

Figure (2b) Photograph of the M910 TPDS-T Sabot, Pusher and Sub-Projectile

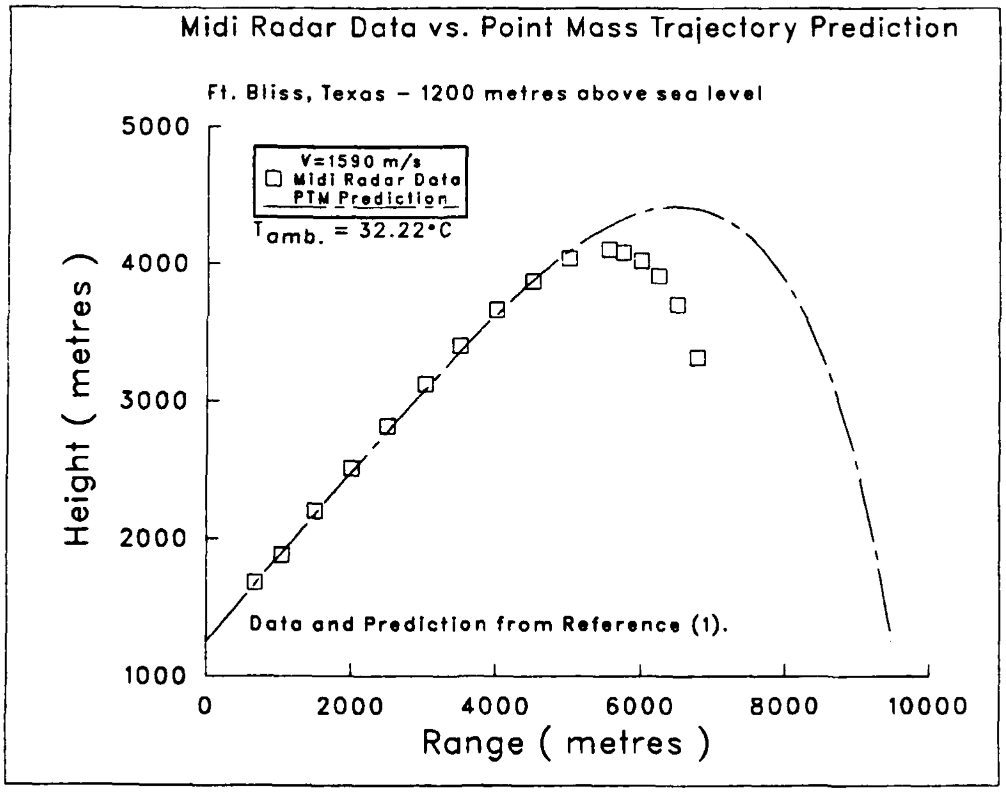

Figure (3) Ft. Bliss, Texas, Midi Radar Data versus Point Mass Trajectory Prediction

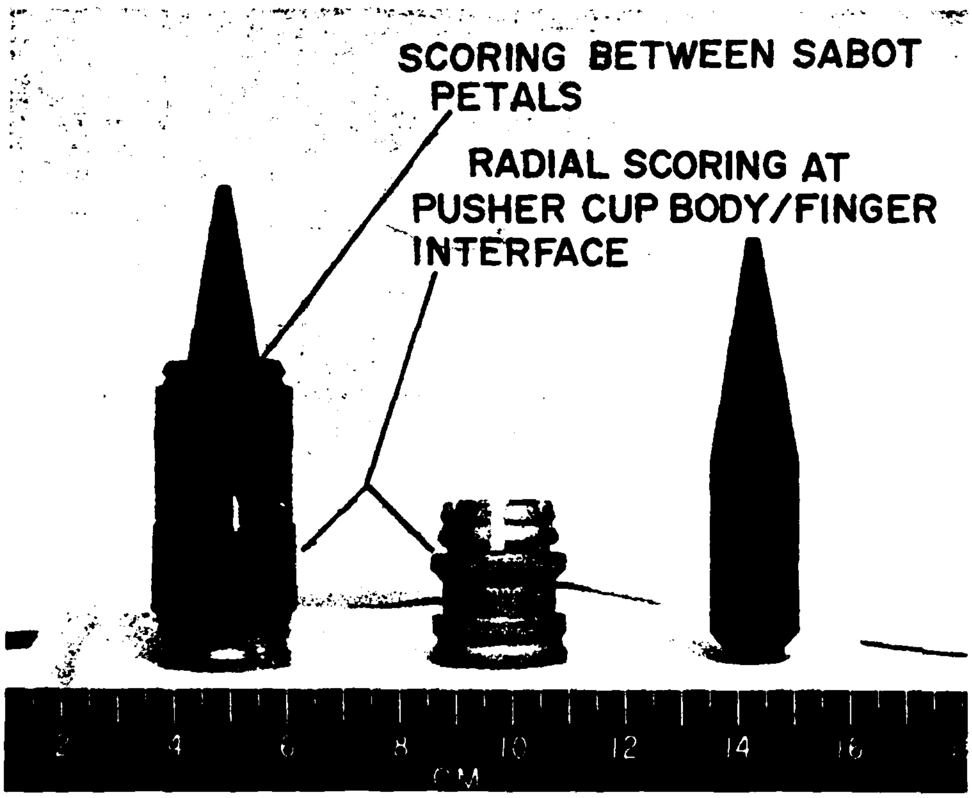

Figure (4) Sabot Modifications

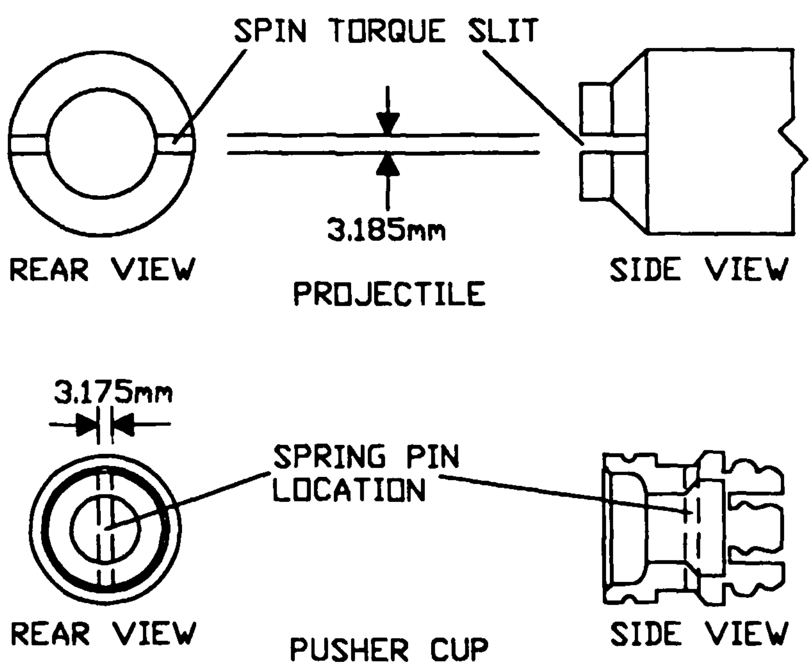

Figure (5) Pusher Modifications

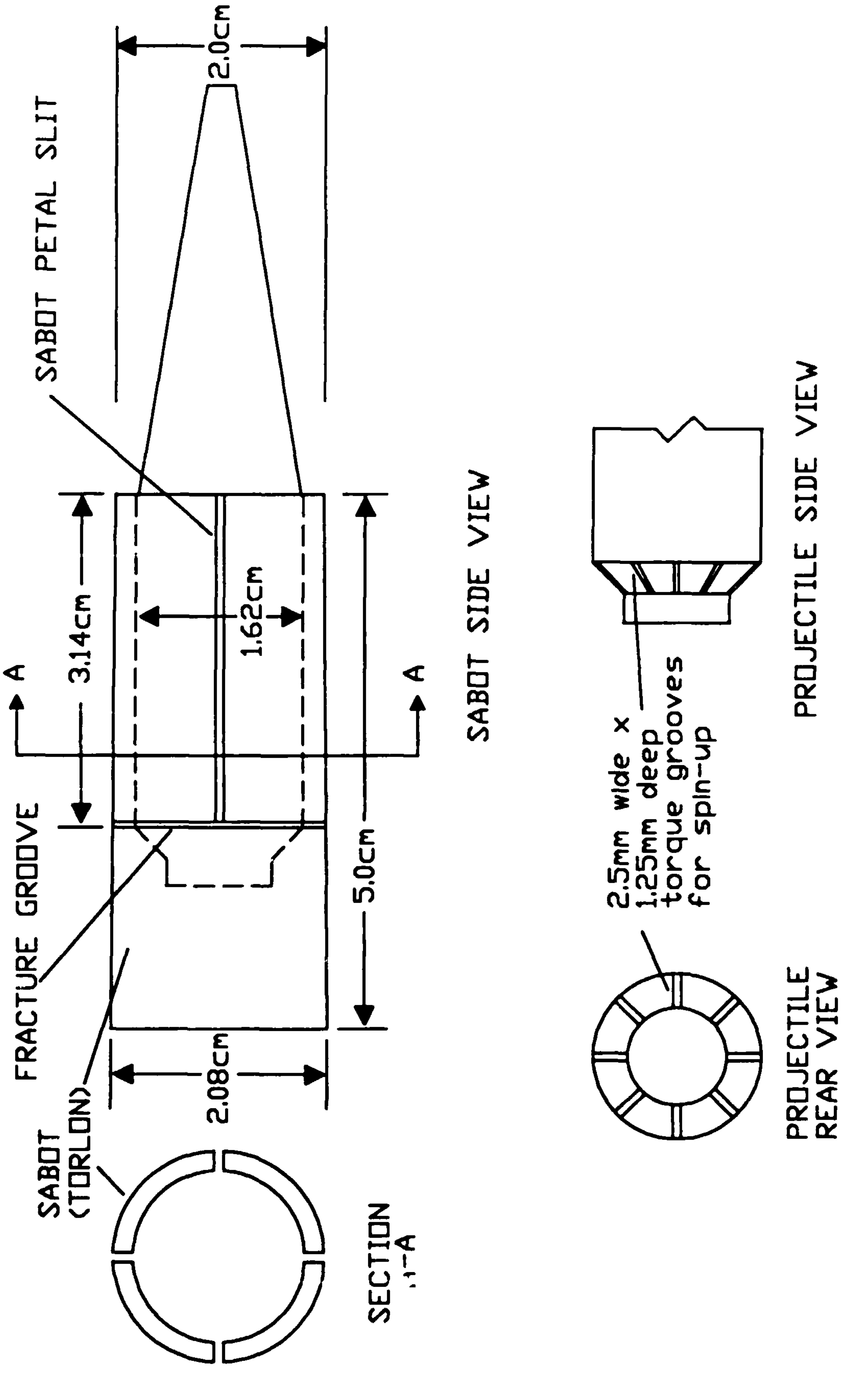

Figure (6) 20 mm Sabot for the M910 TPDS-T and Sub-Projectile Modifications

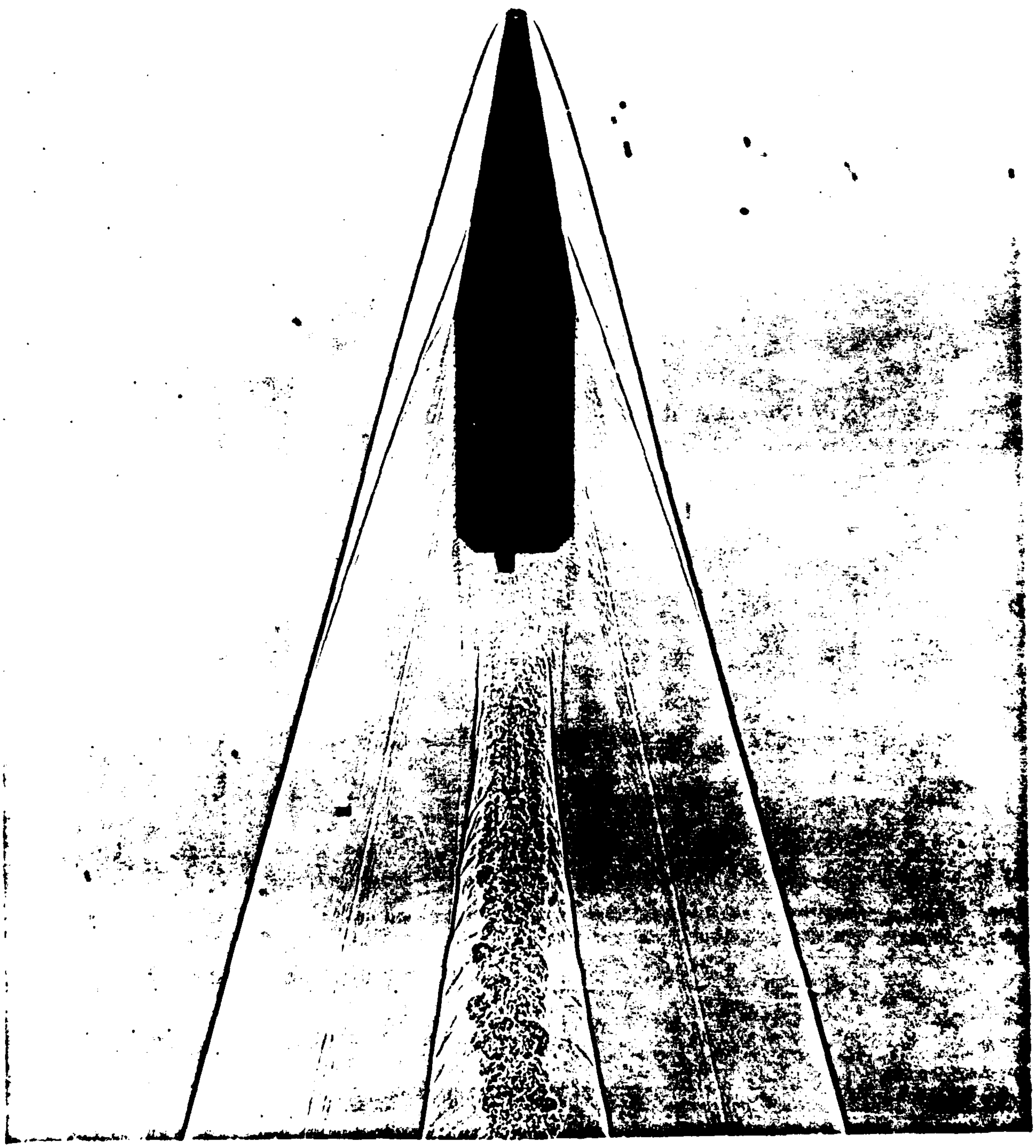

Horizontal View, α = -0.84 deg., β = 0.15 deg.

Figure (7a) Supersonic Flow Field Shadowgraph: M_{∞} = 4.49

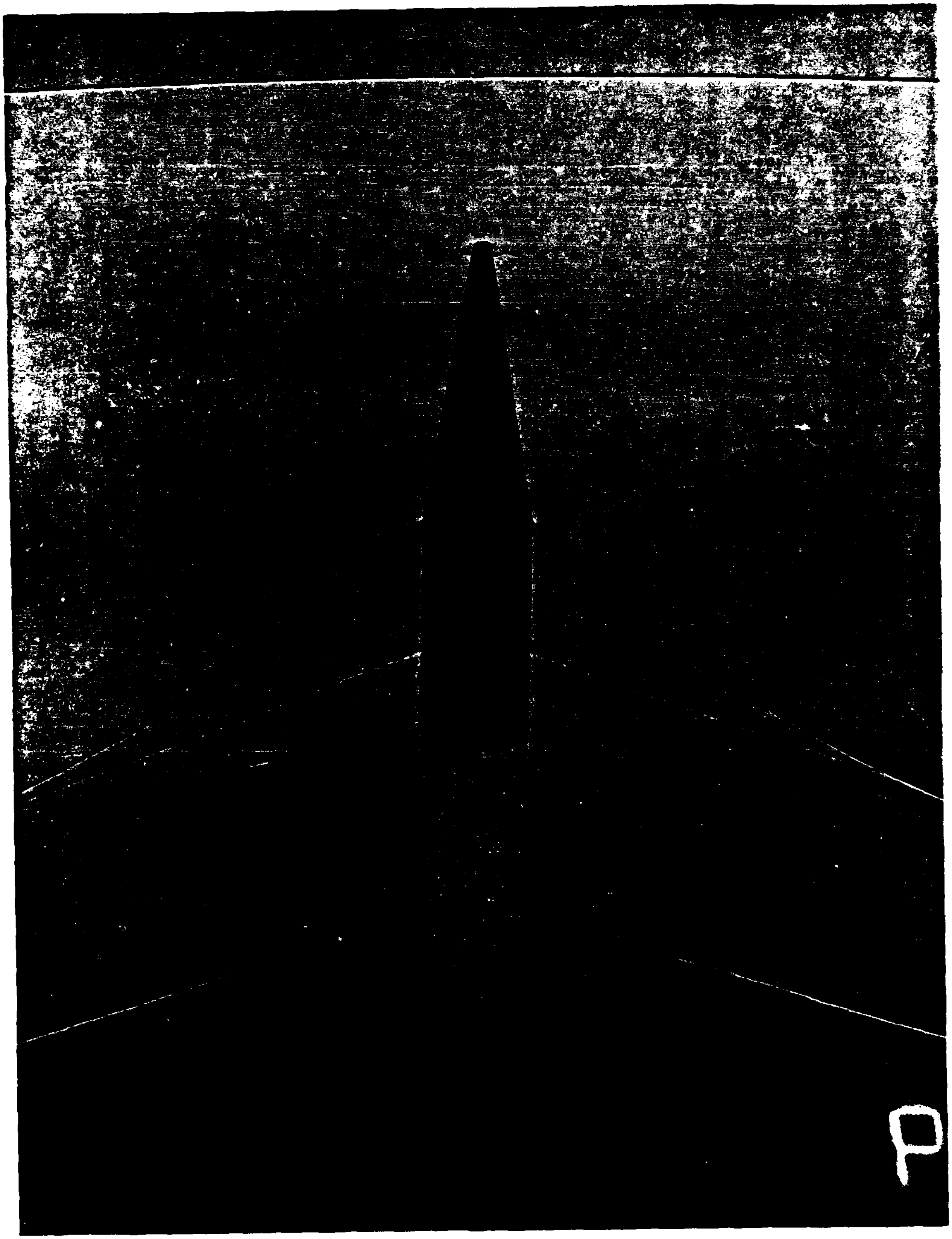

Vertical View, α = 1.43 deg., β = -0.022 deg.

Figure (7b) Transonic Flow Field Shadowgraph: M_{∞} = 1.009

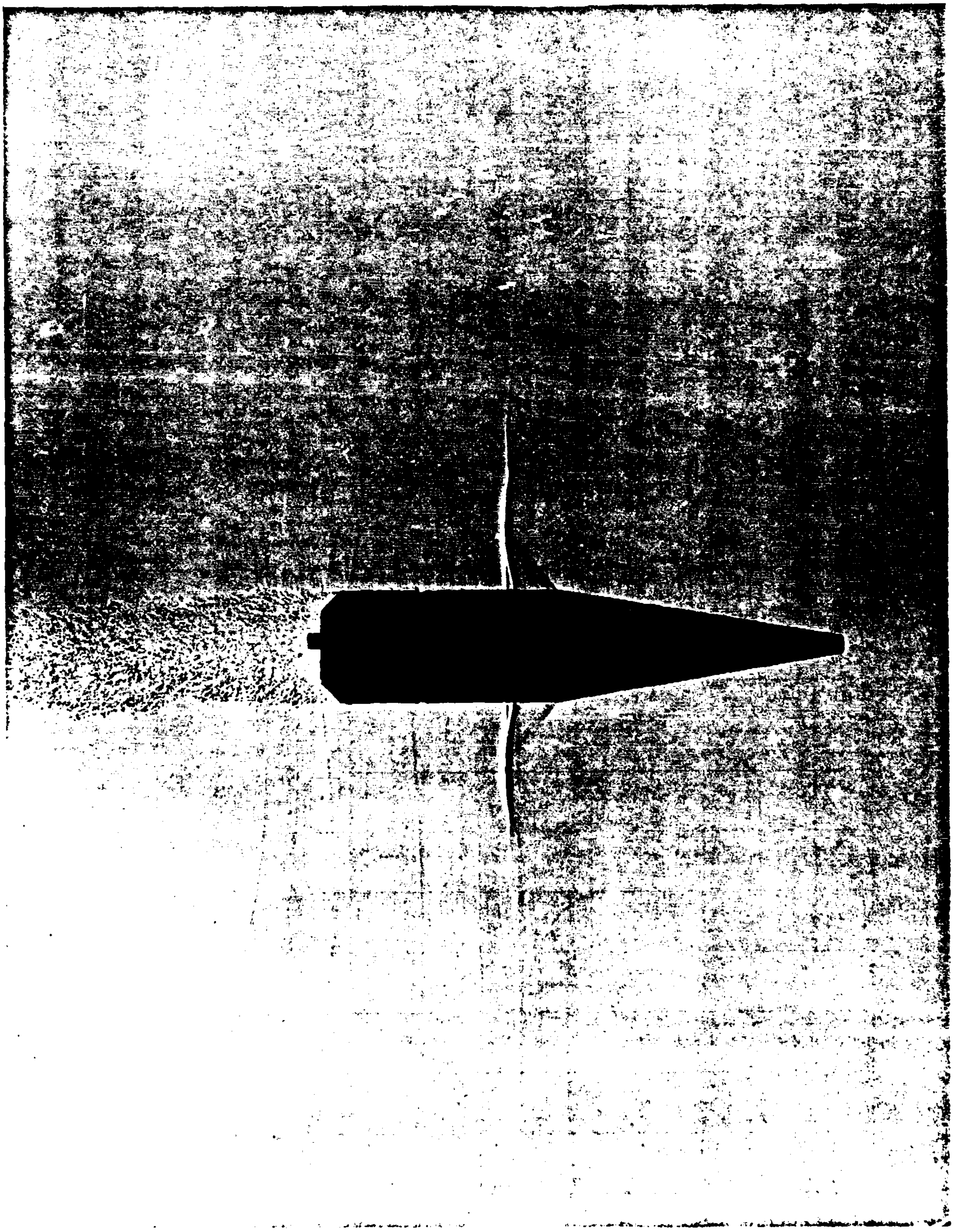

Vertical View, α = -0.54 deg., β = -.014 deg.

Figure (7c) Transonic Flow Field Shadowgraph: M_{∞} = 0.90

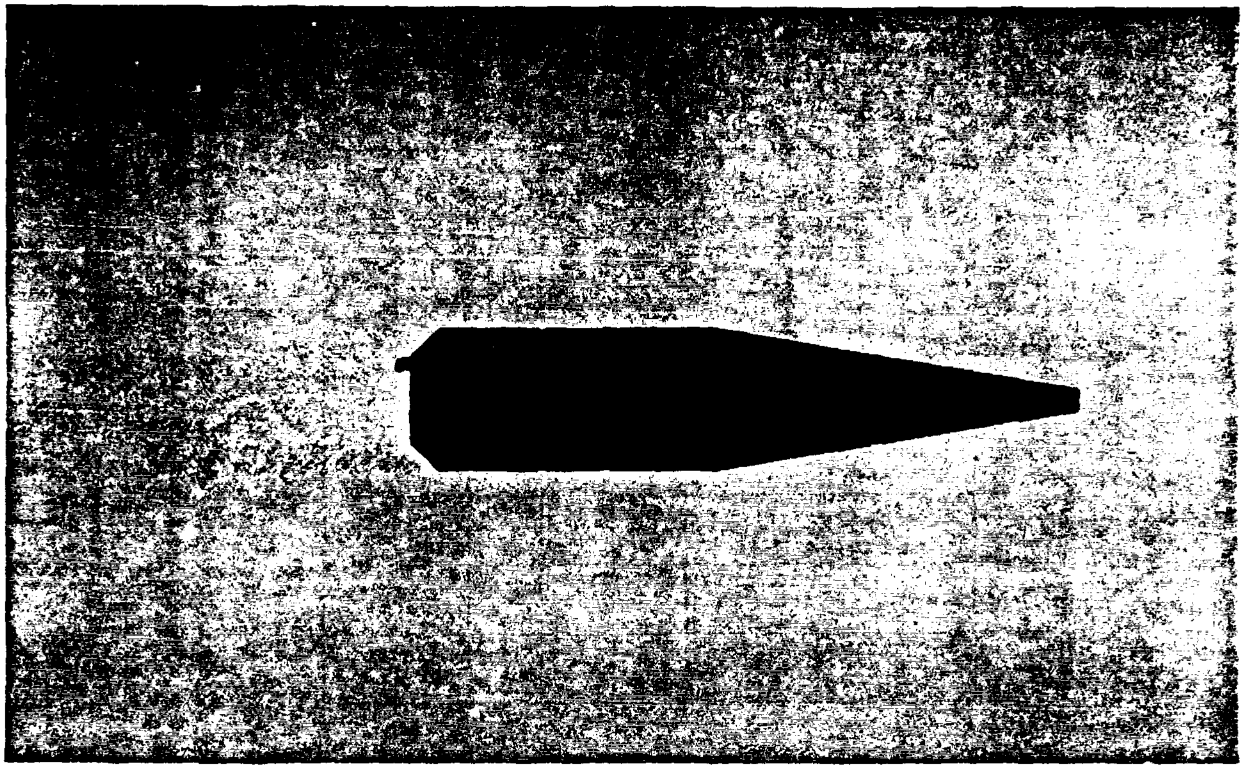

Vertical View, α = -1.04 deg., β = 0.29 deg.

Figure (7d) Subsonic Flow Field Shadowgraph: M_∞ = 0.625

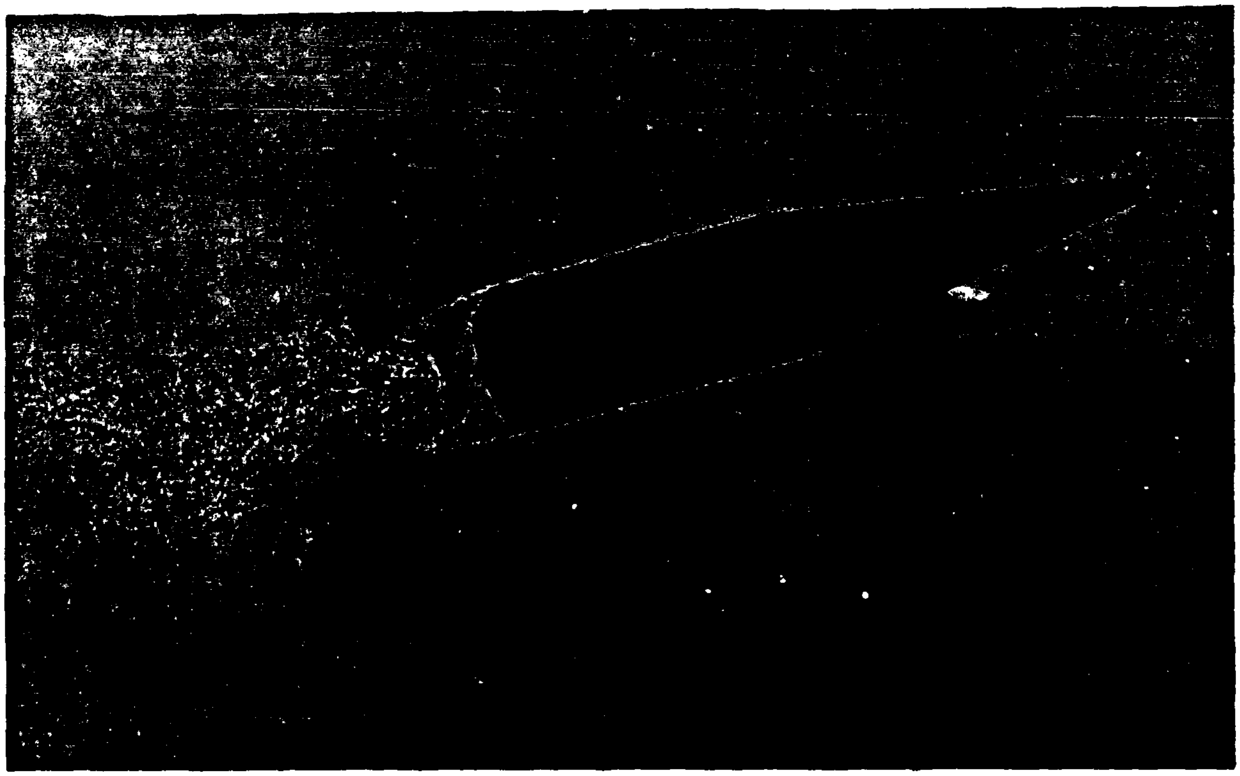

Horizontal View, α = -2.35 deg., β = 15.31 deg.

Figure (7e) High Yaw Subsonic Flow Field Shadowgraph: M_∞ = 0.62

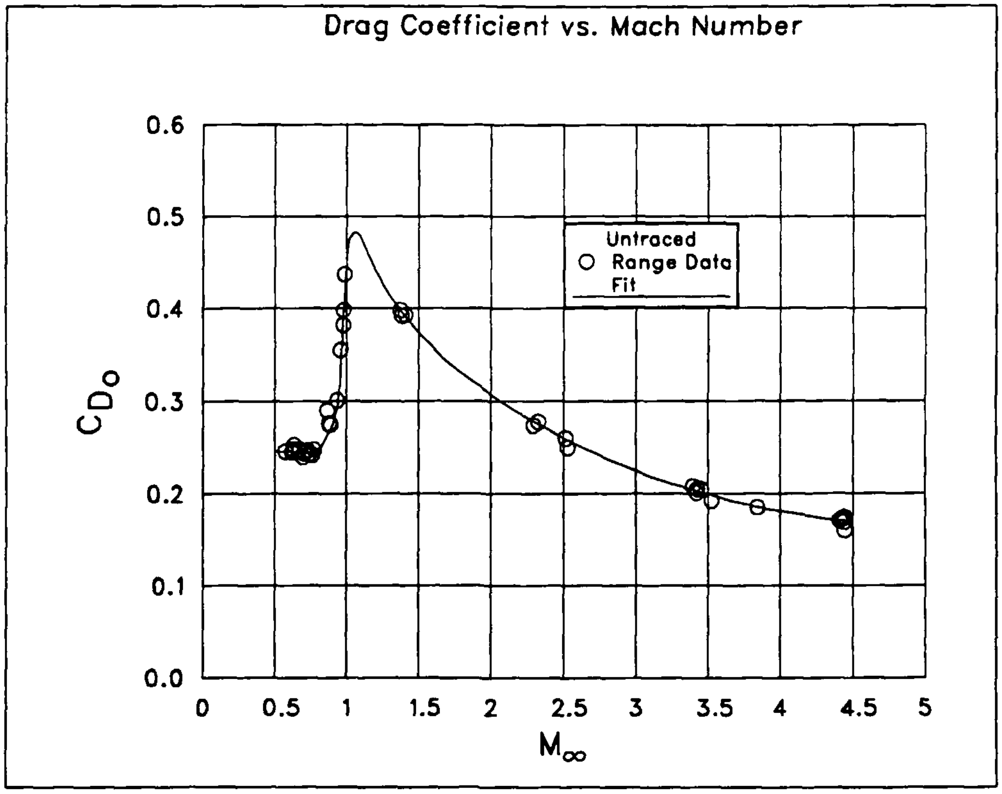

Figure (8a) Zero-Yaw Drag Coefficient versus Mach Number

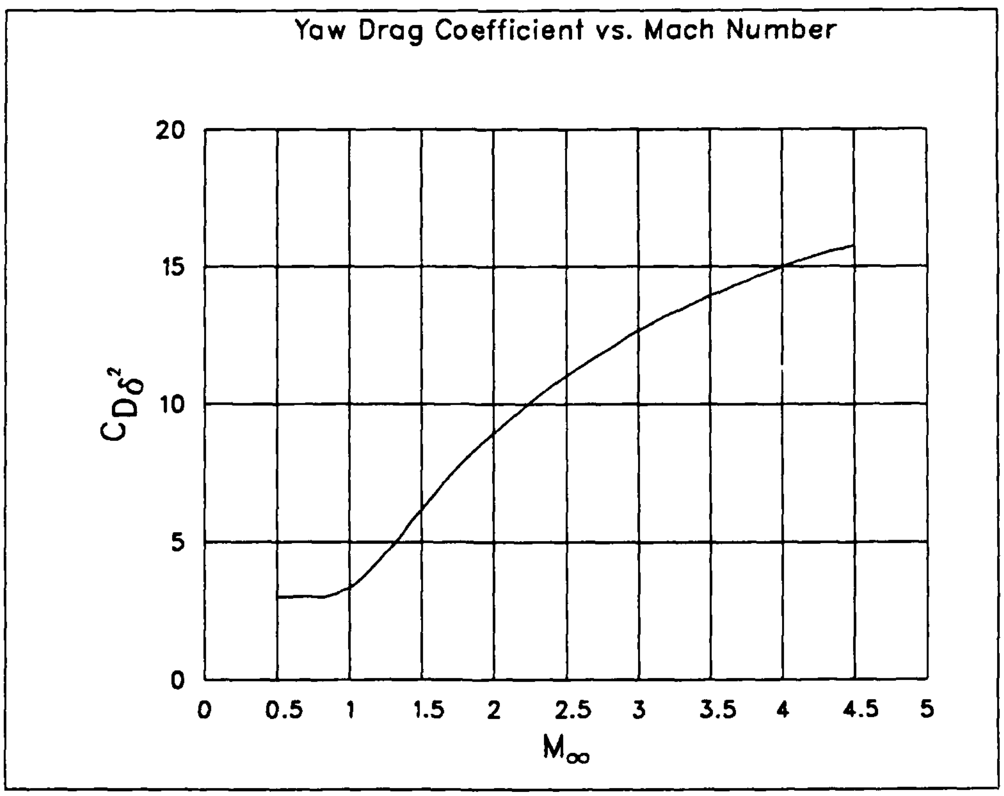

Figure (8b) Quadratic-Yaw Drag Coefficient versus Mach Number

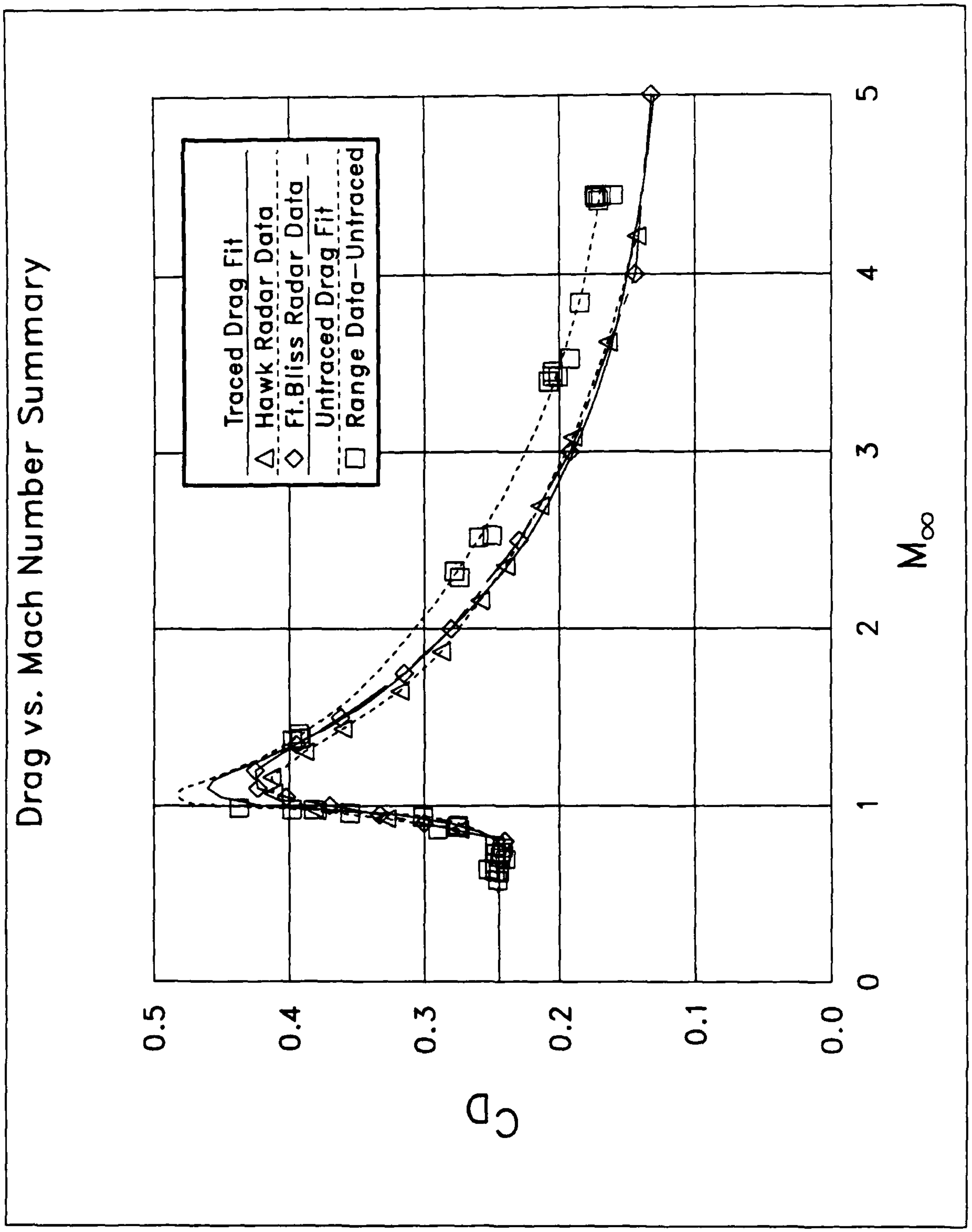

Figure (9) Drag Coefficient Data Summary

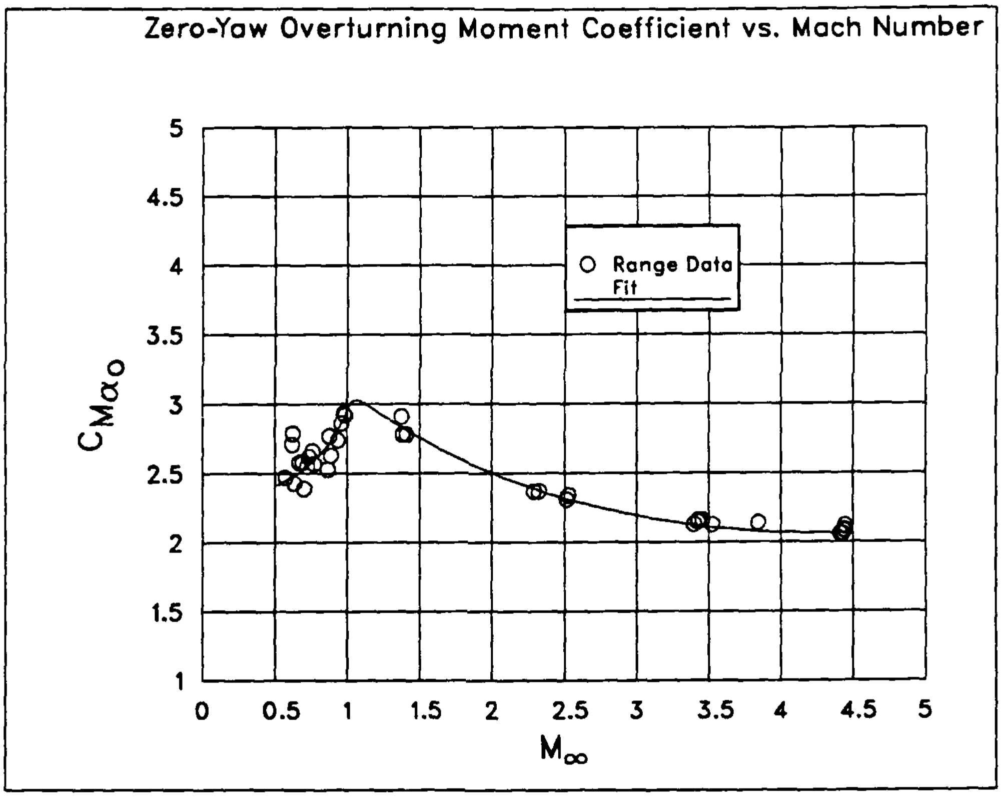

Figure (10a) Zero-Yaw Overturning Moment Coefficient versus Mach Number

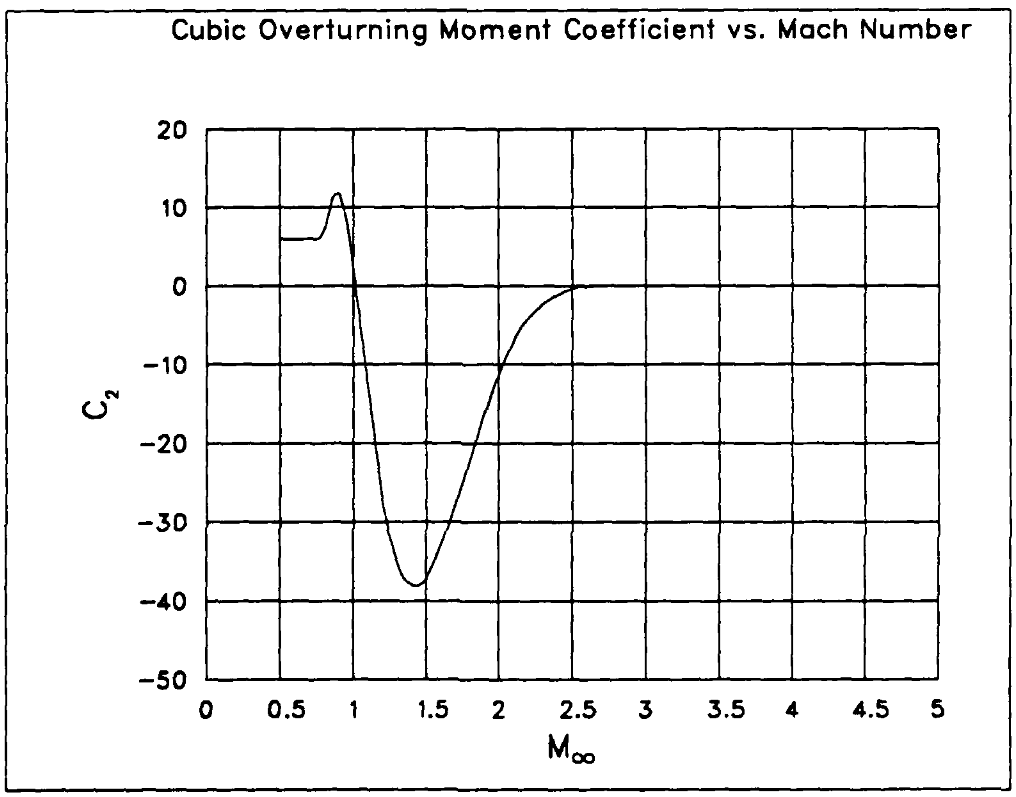

Figure (10b) Cubic Overturning Moment Coefficient versus Mach Number

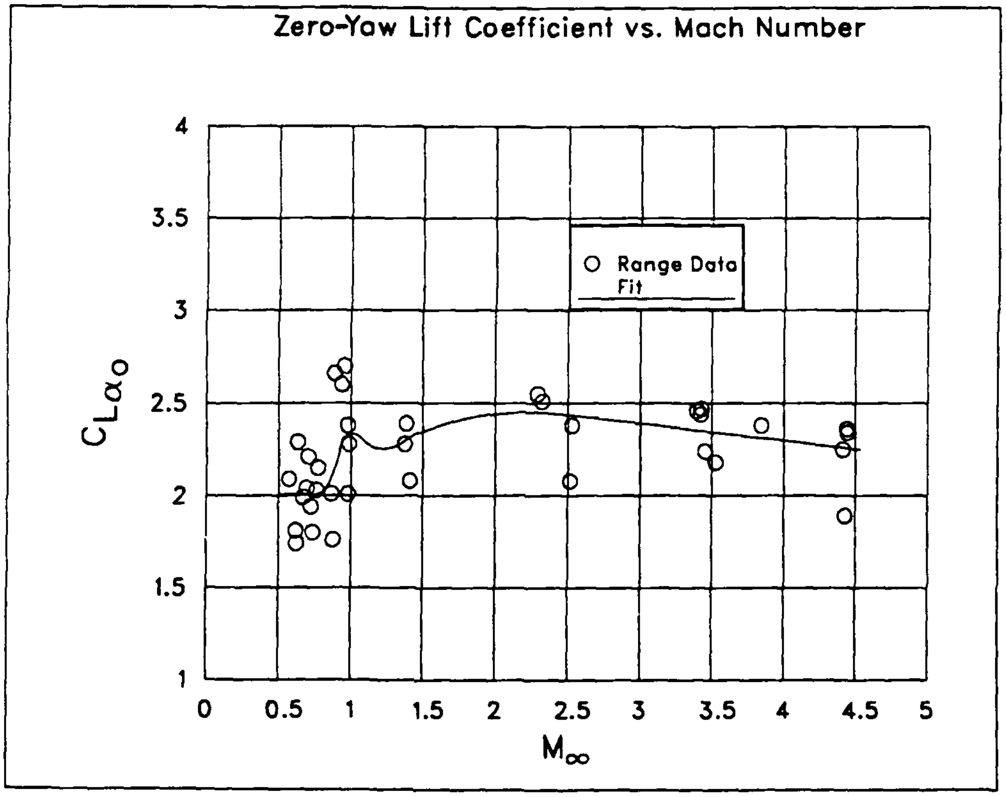

Figure (11a) Zero-Yaw Lift Coefficient versus Mach Number

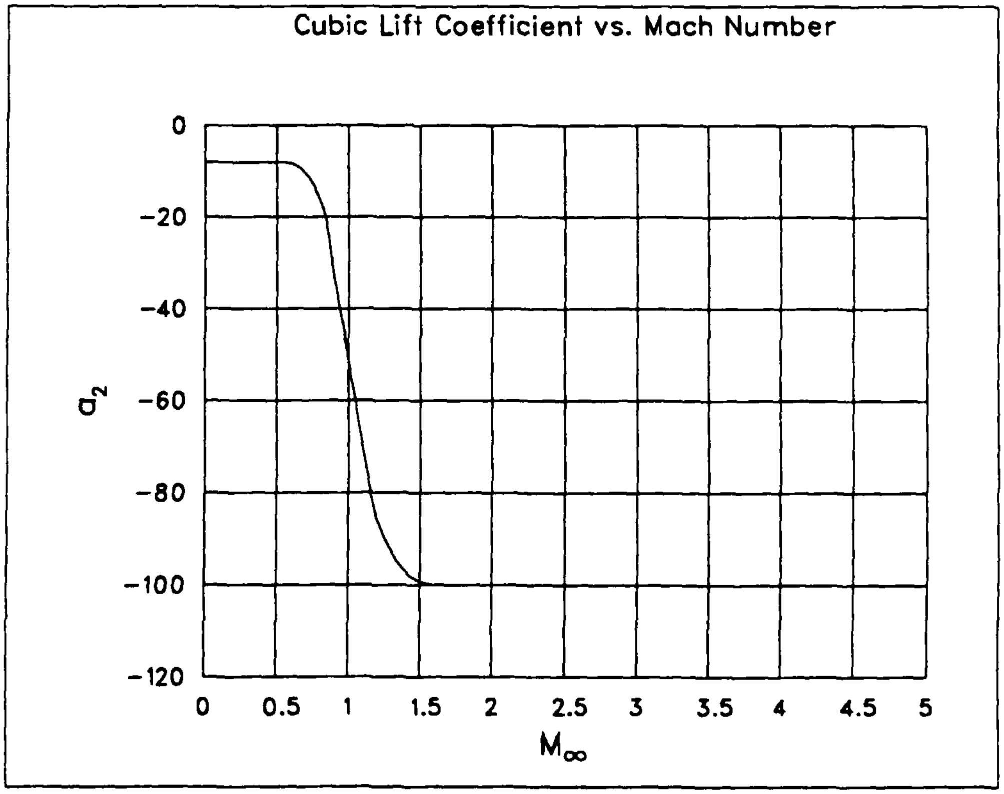

Figure (11b) Cubic Lift Coefficient versus Mach Number

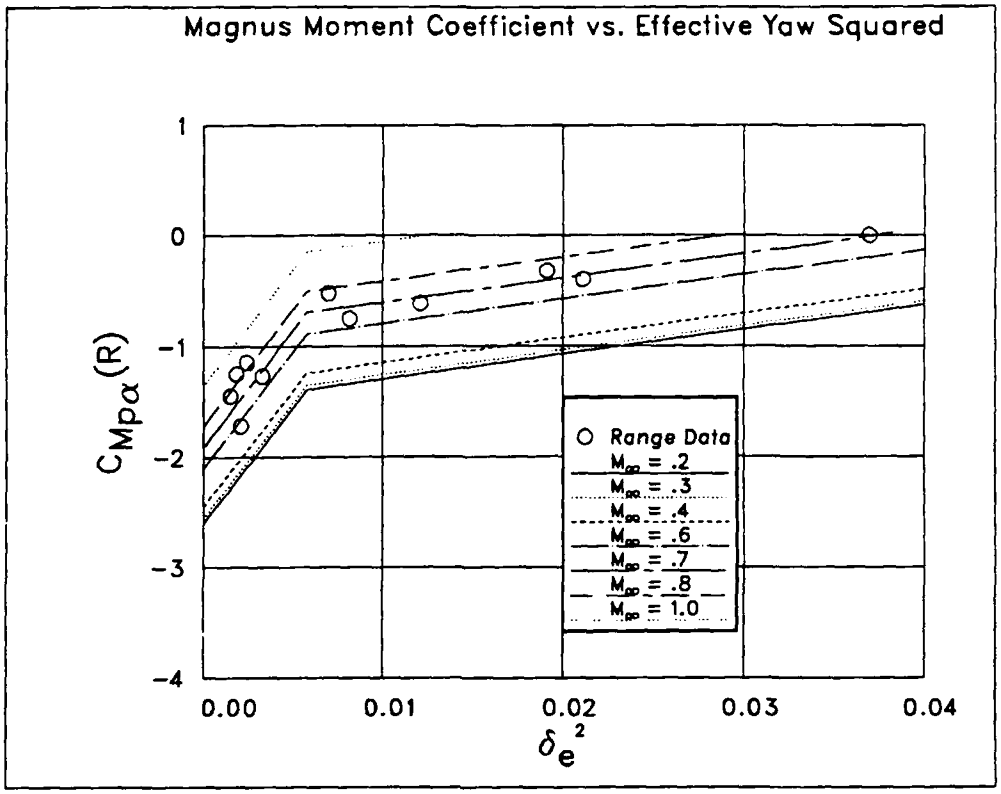

Figure (12a) Magnus Moment Coefficient versus Effective Yaw Squared

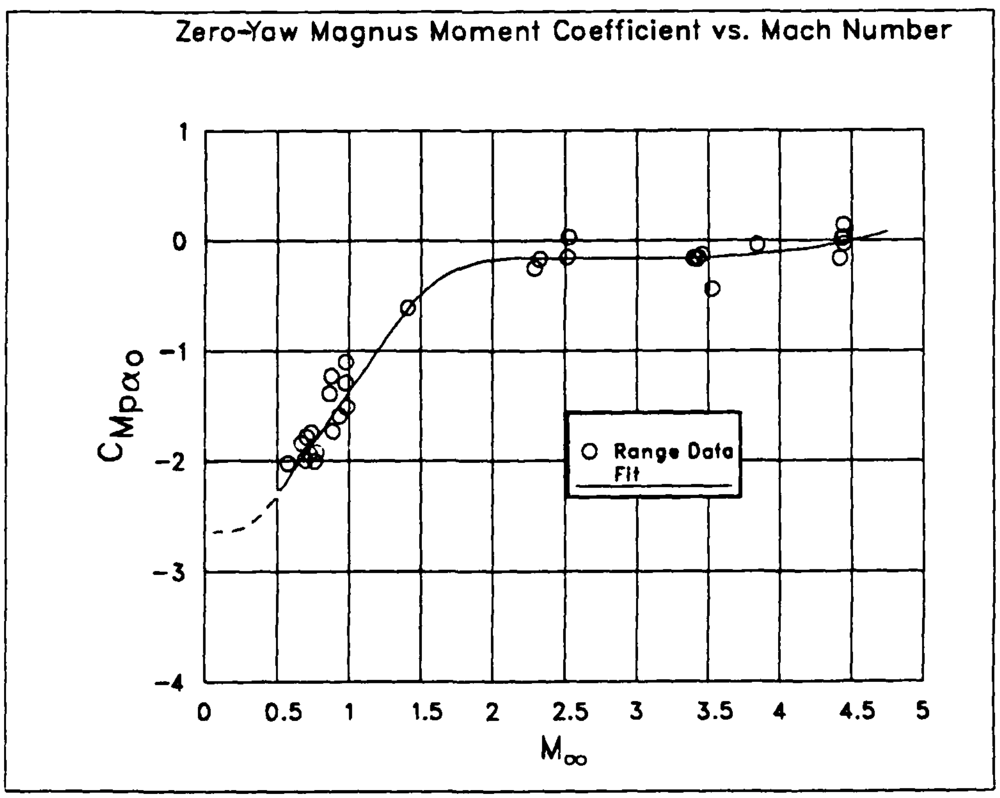

Figure (12b) Zero-Yaw Magnus Moment Coefficient versus Mach Number

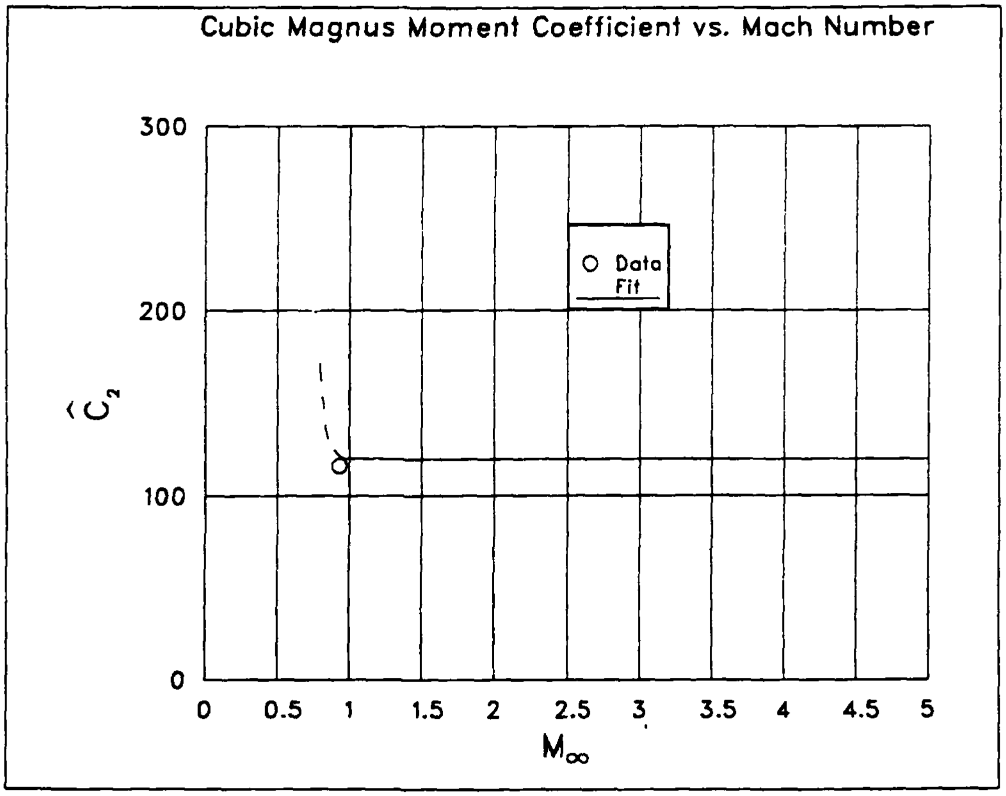

Figure (12c) Cubic Magnus Moment Coefficient versus Mach Number

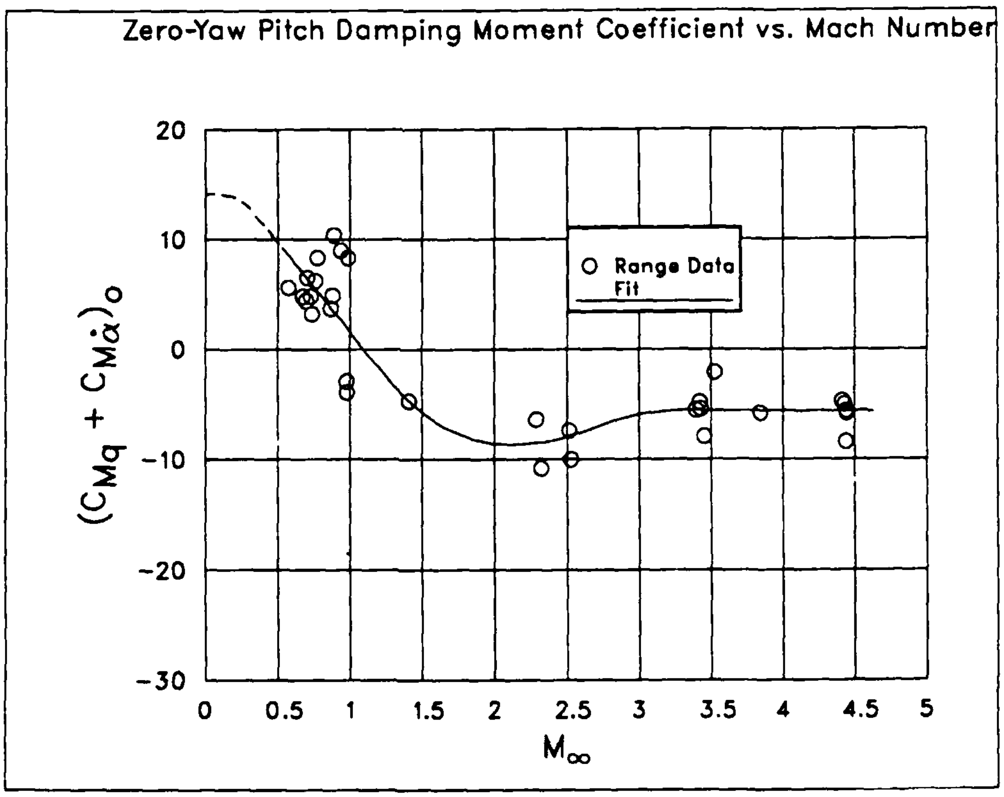

Figure (13a) Zero-Yaw Pitch Damping Moment Coefficient versus Mach Number

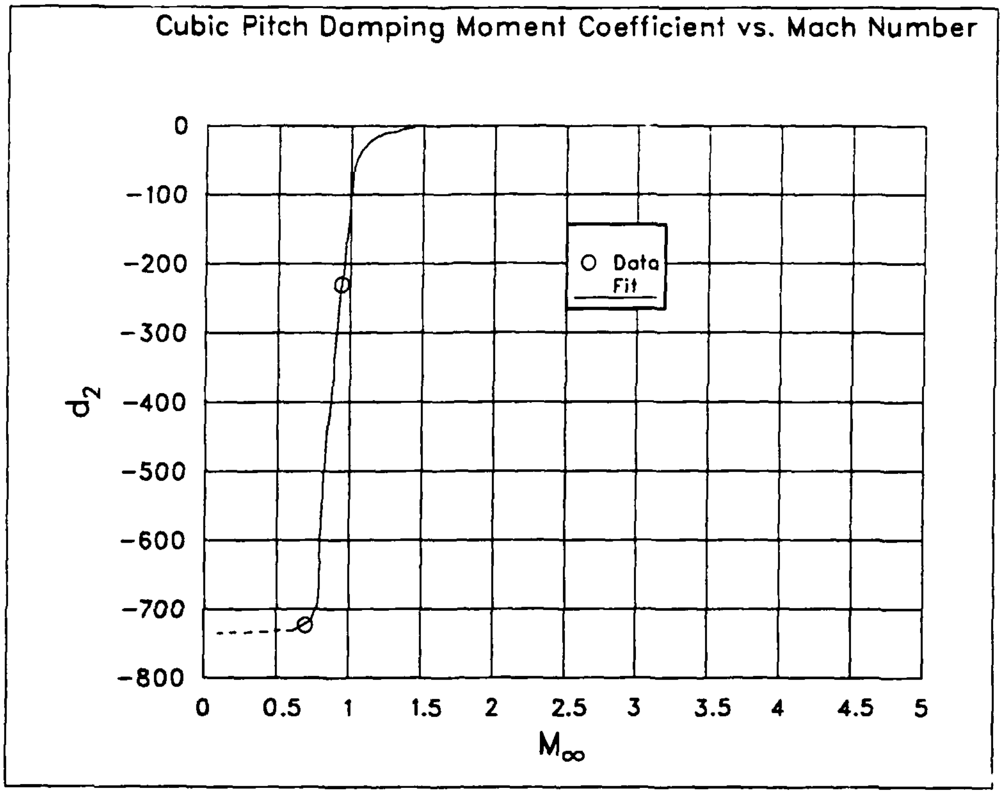

Figure (13b) Cubic Pitch Damping Moment Coefficient versus Mach Number

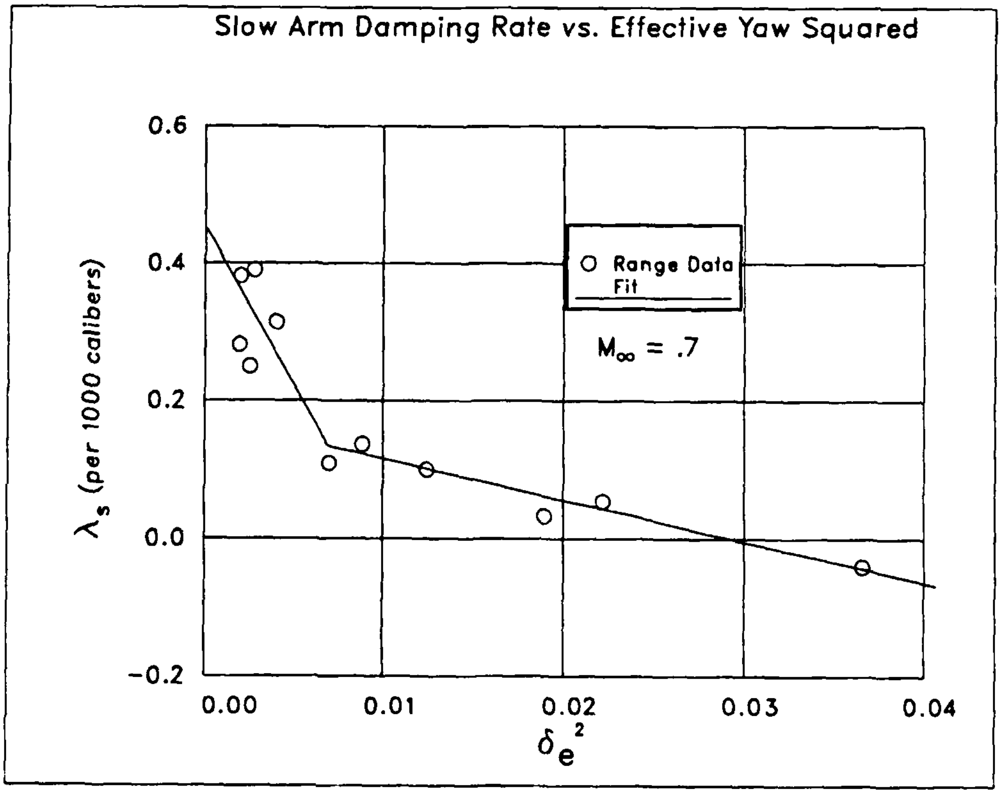

Figure (14a) Slow Arm Damping Rate versus Effective Yaw Squared: $M_\infty = 0.70$

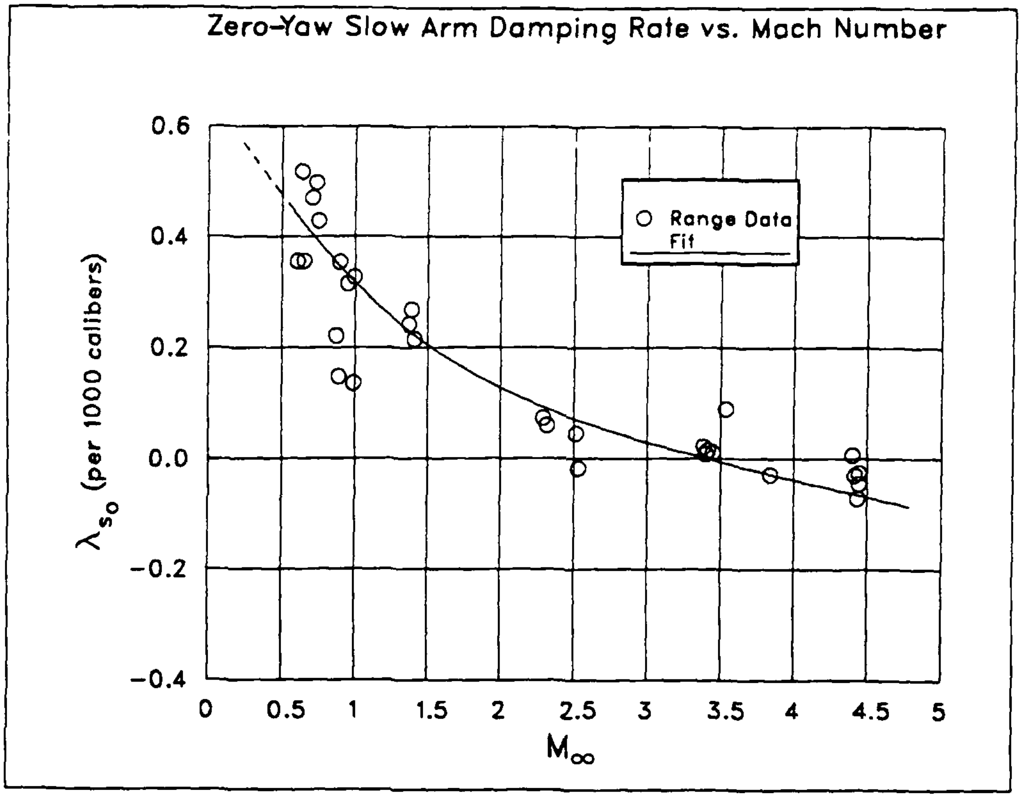

Figure (14b) Zero-Yaw Slow Arm Damping Rate versus Mach Number

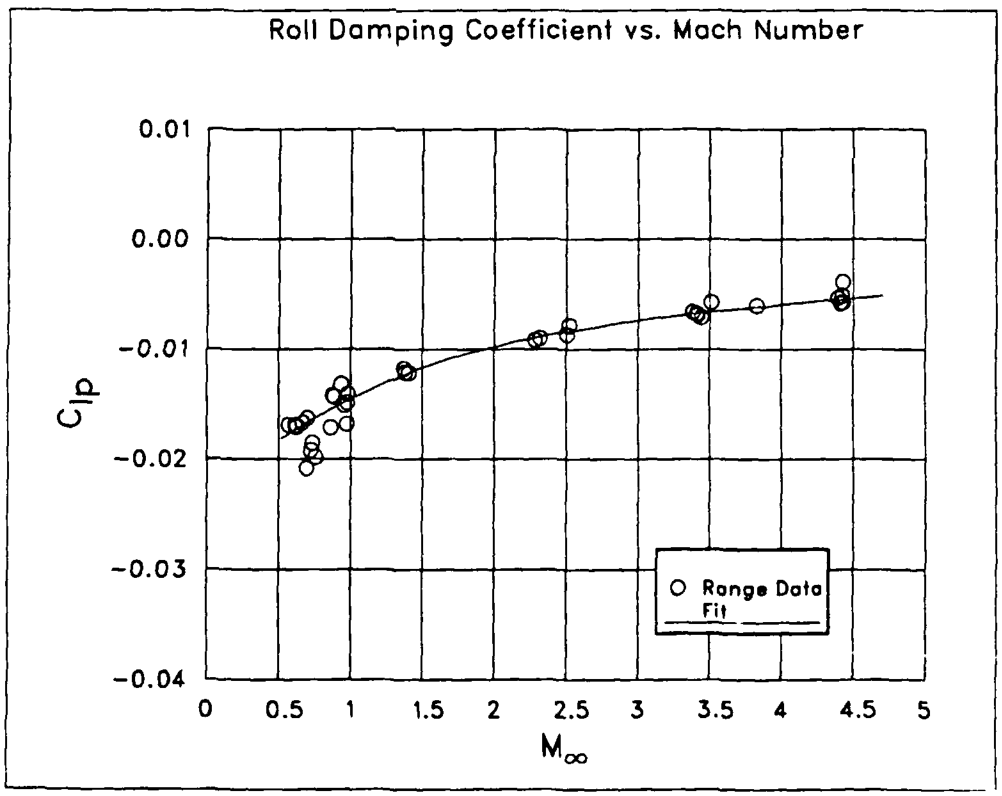

Figure (15) Spin Damping Moment Coefficient versus Mach Number

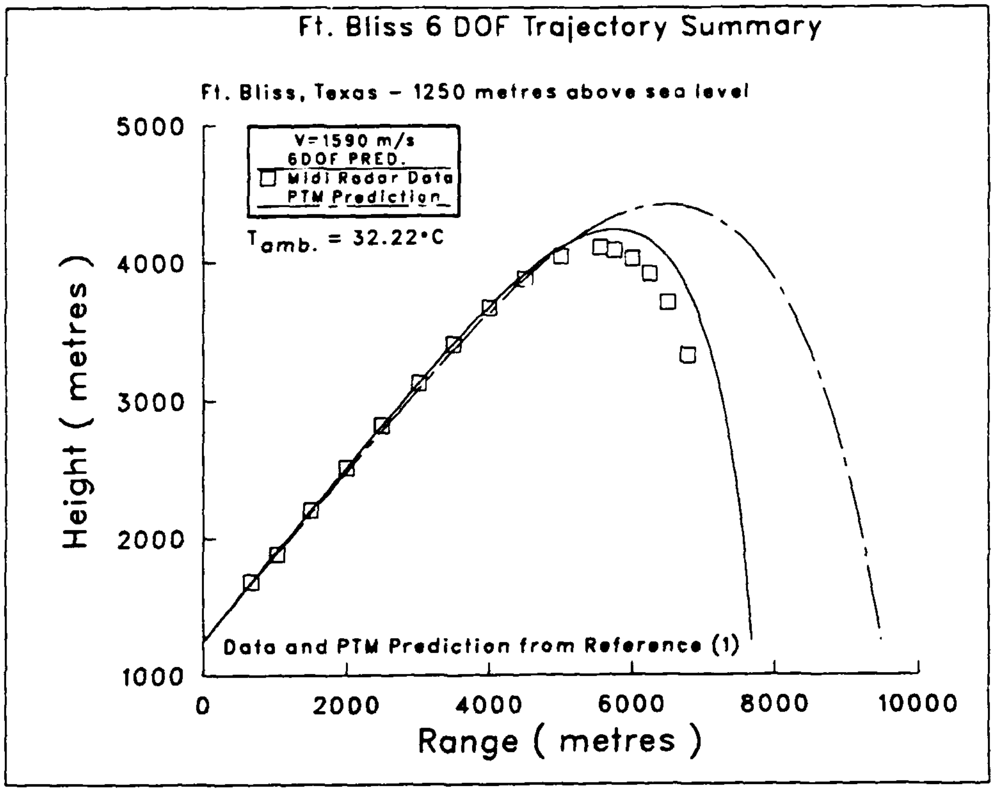

Figure (16) Ft. Bliss 6 Degree-of-Freedom Trajectory

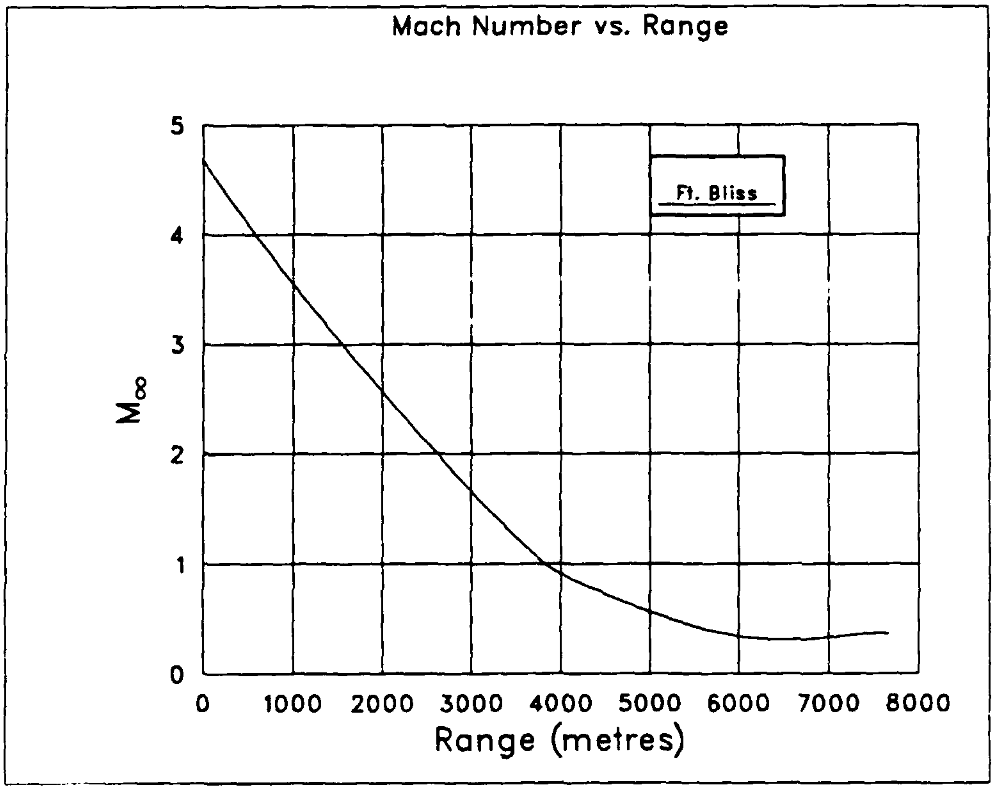

Figure (17) Ft. Bliss Trajectory: Mach Number versus Range

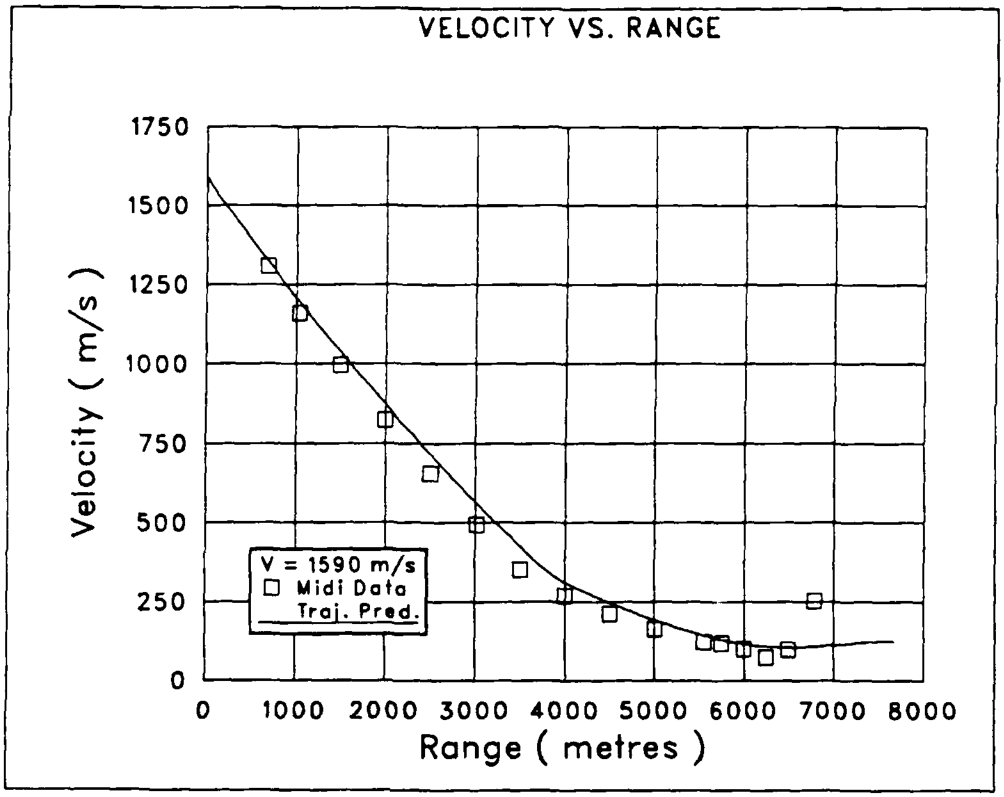

Figure (18) Ft. Bliss Trajectory: Velocity versus Range

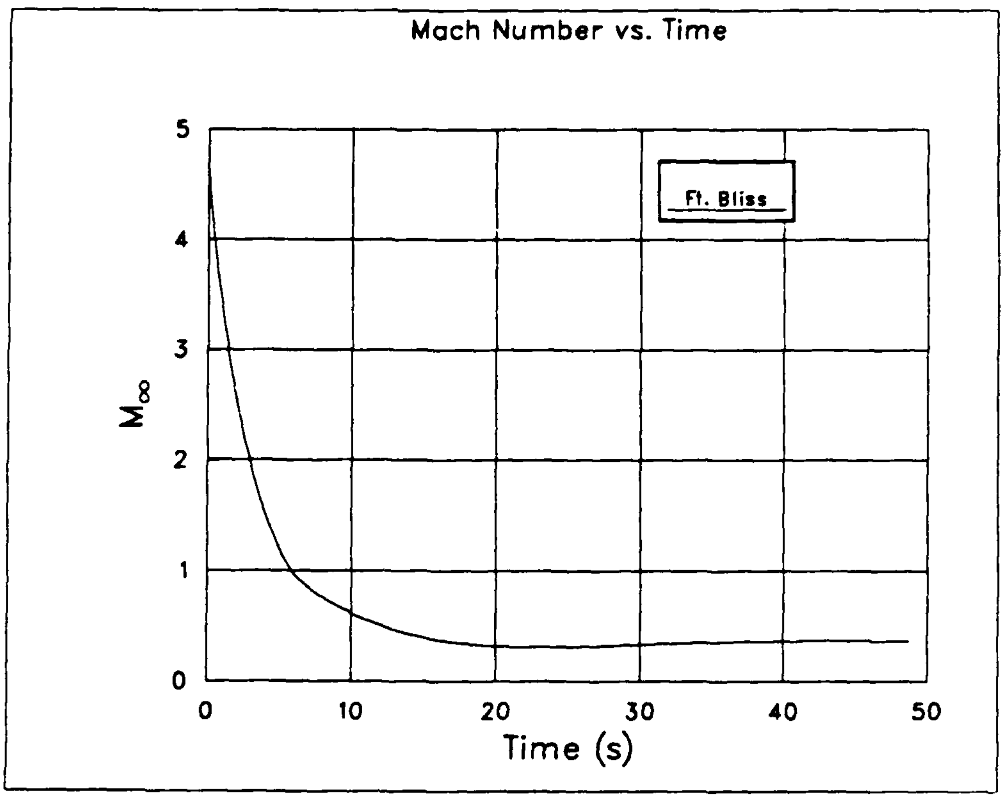

Figure (19) Ft. Bliss Trajectory: Mach Number versus Time

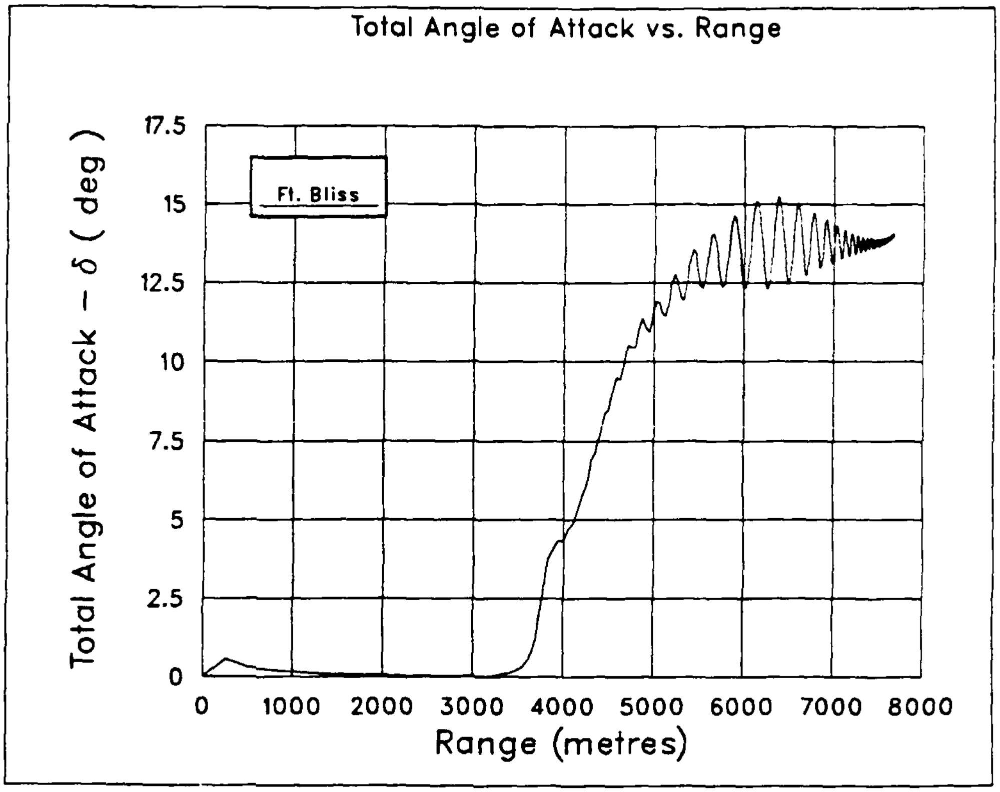

Figure (20) Ft. Bliss Trajectory: Total Angle of Attack versus Range

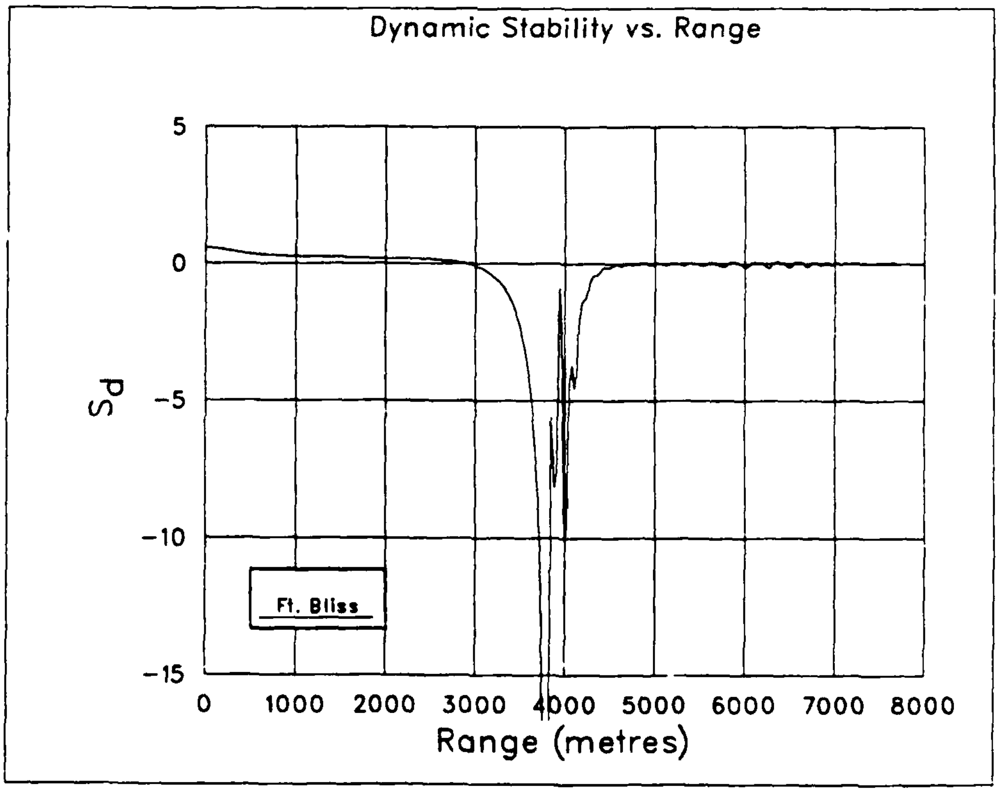

Figure (21) Ft. Bliss Trajectory: Dynamic Stability versus Range

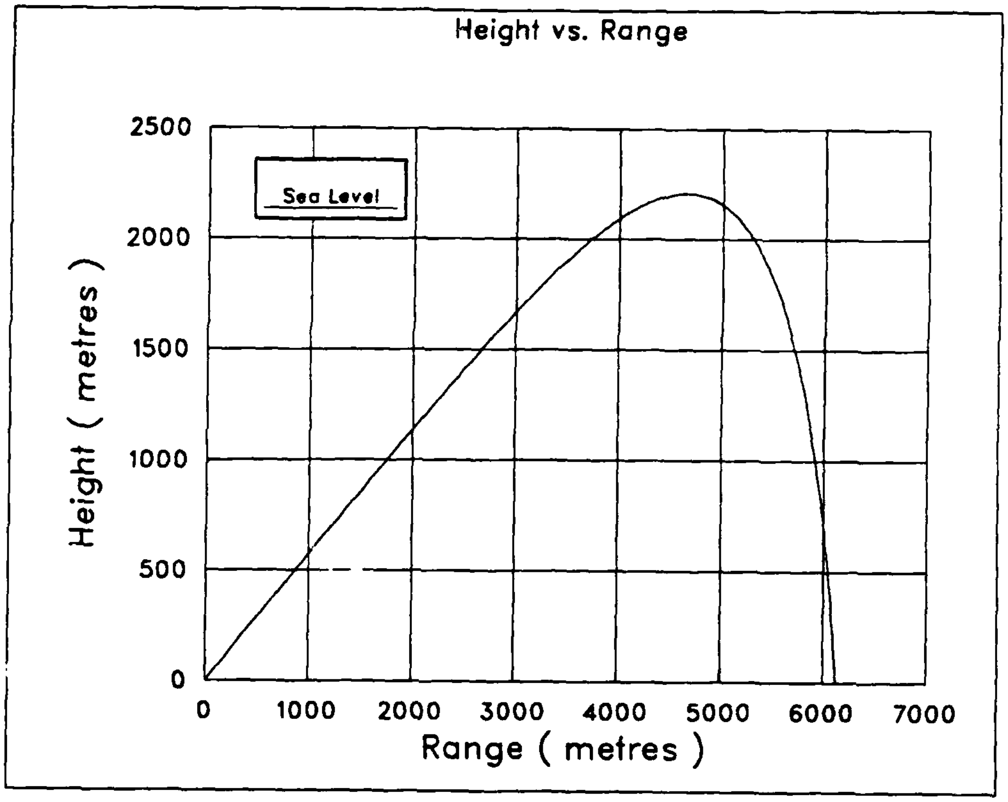

Figure (22) Sea Level Trajectory: Height versus Range

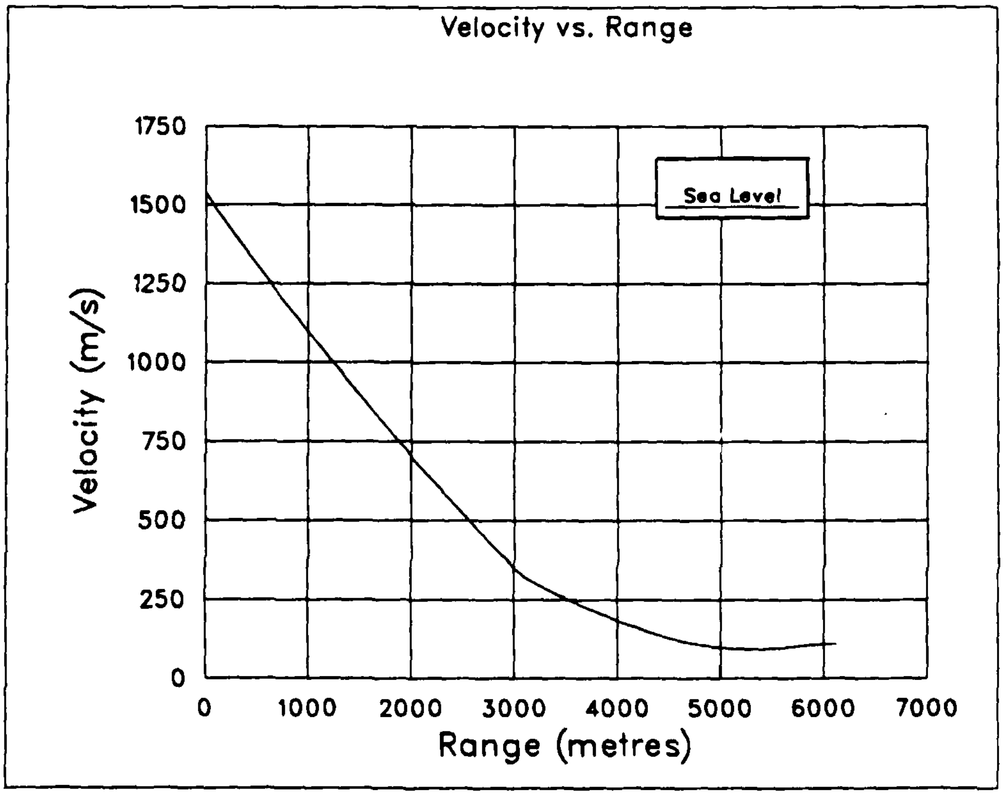

Figure (23) Sea Level Trajectory: Velocity versus Range

Table (1) Projectile Physical Properties of the M910 TPDS-T

Diameter (cm)	1.62
Length (cm)	7.59
Weight (gms)	66.90
Center of Gravity (cm from the nose)	4.47
Axial Moment of Inertia (gm-cm^2)	21.57
Transverse Moment of Inertia (gm-cm^2)	146.87

Table (2) Range Values of Aerodynamic Coefficients of the M910 APTP-T

Round No.	Mach No.	α_T (Degrees)	C_D	$C_{M\alpha}$	$C_{L\alpha}$	$C_{Mp\alpha}$	$C_{Mq}+C_{M\dot{\alpha}}$	C_{PN} (cal-base)	C_{lp}
19002	4.44	1.51	0.170	2.12	2.27	0.07	-5.48	2.94	-0.0039
19017	4.44	1.49	0.184	2.08	2.25	0.14	-5.75	2.78	-0.0058
19001	4.44	0.45	0.169	2.09	2.35	0.15	-8.39	2.75	-0.0052
19000	4.43	1.38	0.181	2.06	1.82	0.10	-4.80	2.96	-0.0059
19053	4.41	0.94	0.175	2.06	2.25	-0.12	-4.61	2.77	-0.0054
19003	3.84	1.45	0.194	2.14	2.37	0.04	-5.40	2.76	-0.0061
19052	3.53	0.94	0.196	2.13	2.15	-0.41	-1.91	2.83	-0.0058
19005	3.45	0.64	0.207	2.16	2.23	-0.11	-7.48	2.81	-0.0071
19018	3.43	1.87	0.219	2.15	2.34	-0.01	-5.12	2.76	-0.0069
19004	3.42	1.60	0.211	2.15	2.35	-0.08	-4.22	2.76	-0.0068
19006	3.40	1.45	0.216	2.13	2.38	-0.06	-5.52	2.74	-0.0067
19008	2.53	0.90	0.252	2.34	2.36	0.05	-9.78	2.82	-0.0079
19019	2.52	1.86	0.271	2.31	2.07	-0.03	-6.65	2.91	-0.0087
19007	2.33	1.22	0.282	2.37	2.47	-0.13	-10.35	2.78	-0.0090
19009	2.29	2.69	0.296	2.37	2.29	0.04	-5.30	2.84	-0.0092
19013	1.41	3.01	0.408	2.69	1.78	-0.32	-2.16	3.15	-0.0121
19014	1.38	2.18	0.399	2.75	2.27			2.95	-0.0121
19015	1.37	2.33	0.406	2.87	2.13			3.06	-0.0118
19049	0.99	2.55	0.442	2.92	2.20	-1.37	9.66	3.03	-0.0141
19037	0.98	4.40	0.417	2.96	1.70	-0.47	-1.02	3.32	-0.0168
19038	0.98	4.57	0.403	2.98	2.02			3.16	-0.0149
19039	0.96	6.52	0.396	2.96	2.11			3.11	-0.0151
19040	0.94	2.65	0.307	2.76	2.52	-1.38	9.81	2.90	-0.0132
19048	0.89	2.65	0.281	2.65	2.60	-1.53	11.24	2.84	-0.0143
19046	0.88	3.32	0.287	2.83	1.63	-0.72	4.64	3.40	-0.0142
19036	0.87	3.58	0.301	2.57	1.90	-0.95	5.13	3.09	-0.0171
19032	0.77	8.98	0.321	2.78	1.64	0.00	-2.36	3.34	-0.0263
19033	0.76	5.37	0.268	2.73	1.87	-0.62	5.23	3.20	-0.0198
19034	0.74	3.95	0.257	2.66	1.73	-0.52	1.64	3.27	-0.0185
19035	0.73	3.47	0.257	2.57	1.89	-1.27	7.27	3.12	-0.0192

Table (2) Range Values of Aerodynamic Coefficients of the M910 APTP-T
(continued)

Round No.	Mach No.	α_T (Degrees)	C_D	$C_{M\alpha}$	$C_{L\alpha}$	$C_{Mp\alpha}$	$C_{Mq}+C_{M\dot{\alpha}}$	C_{PN} (cal-base)	C_{lp}
19045	0.70	2.70	0.250	2.40	2.19	-1.45	8.61	2.91	-0.0163
19025	0.69	7.05	0.285	2.70	1.82	-0.40	2.14	3.36	-0.0208
19042	0.67	6.59	0.288	2.69	1.84	-0.33	1.53	3.19	-0.0167
19041	0.63	3.12	0.261	2.44	2.27	-1.72	16.05	2.89	-0.0170
19068	0.63	2.54	0.254	2.80	1.73	-1.25	-13.26	3.34	-0.0171
19066	0.62	2.91	0.253	2.72	1.79	-1.15	-12.01	3.25	-0.0169
19029	0.62								-0.0689
19028	0.58								-0.1117
19044	0.57	4.67	0.265	2.52	2.02	-0.77	6.89	3.03	-0.0169

Table (3) Range Values of Flight Motion Parameters of the M910 APTP-T

Round No.	S_g	S_d	$\lambda_F x10^3$ (1/cal)	$\lambda_S x10^3$ (1/cal)	K_F	K_S	$\phi'_F x10^2$ (rad/cal)	$\phi'_S x10^2$ (rad/cal)	Spin (rad/cal)
19002	2.15	0.64	-0.196	-0.069	0.0160	0.0195	2.164	0.346	0.173
19017	2.16	0.75	-0.188	-0.089	0.0167	0.0184	2.317	0.321	0.173
19001	2.16	0.58	-0.288	-0.079	0.0039	0.0062	2.233	0.332	0.172
19000	2.18	0.69	-0.164	-0.065	0.0131	0.0194	2.212	0.330	0.172
19053	2.15	0.32	-0.228	-0.010	0.0094	0.0126	2.138	0.346	0.172
19003	2.09	0.62	-0.200	-0.063	0.0115	0.0217	2.186	0.347	0.171
19052	2.05	-0.55	-0.210	0.076	0.0065	0.0145	2.111	0.364	0.171
19005	2.03	0.24	-0.344	0.008	0.0060	0.0083	2.164	0.358	0.171
19018	2.06	0.55	-0.209	-0.048	0.0188	0.0250	2.192	0.352	0.171
19004	2.05	0.46	-0.196	-0.029	0.0103	0.0255	2.164	0.357	0.171
19006	2.02	0.43	-0.243	-0.028	0.0165	0.0170	2.145	0.356	0.169
19008	1.92	0.40	-0.396	-0.030	0.0037	0.0149	2.160	0.389	0.173
19019	1.95	0.37	-0.287	-0.016	0.0124	0.0288	2.196	0.377	0.173
19007	1.88	0.19	-0.489	0.039	0.0052	0.0198	2.152	0.395	0.172
19009	1.89	0.62	-0.205	-0.060	0.0235	0.0390	2.167	0.394	0.173
19013	1.70	-0.85	-0.200	0.065	0.0180	0.0481	2.142	0.448	0.174
19014	1.68				0.0021	0.0342	2.103	0.465	0.175
19015	1.63				0.0008	0.0382	2.219	0.460	0.176
19049	1.57	1.88	-0.007	0.330	0.0075	0.0390	2.168	0.486	0.175
19037	1.51	-1.51	-0.199	0.132	0.0346	0.0662	2.062	0.509	0.171
19038	1.56				0.0469	0.0618	2.133	0.496	0.175
19039	1.52				0.0462	0.1026	2.081	0.514	0.174
19040	1.65	1.87	-0.032	0.317	0.0203	0.0373	2.142	0.465	0.175
19048	1.68	1.80	0.004	0.355	0.0189	0.0370	2.164	0.441	0.173
19046	1.57	2.10	-0.031	0.146	0.0402	0.0412	2.208	0.462	0.172
19036	1.81	2.67	-0.082	0.220	0.0294	0.0520	2.185	0.418	0.175
19032	1.51	0.78	-0.098	-0.042	0.1122	0.1070	2.100	0.472	0.166
19033	1.53	1.41	0.028	0.101	0.0612	0.0708	1.999	0.488	0.166
19034	1.57	13.09	-0.102	0.112	0.0480	0.0487	2.058	0.462	0.166
19035	1.74	2.43	-0.097	0.319	0.0232	0.0531	2.154	0.423	0.171

Table (3) Range Values of Flight Motion Parameters of the M910 APTP-T
(continued)

Round No.	S_g	S_d	$\lambda_F x10^3$ (1/cal)	$\lambda_S x10^3$ (1/cal)	K_F	K_S	$\phi'_F x10^2$ (rad/cal)	$\phi'_S x10^2$ (rad/cal)	Spin (rad/cal)
19045	1.85	2.33	-0.087	0.381	0.0088	0.0429	2.121	0.408	0.172
19025	1.63	3.19	-0.037	0.053	0.0811	0.0921	2.143	0.458	0.172
19042	1.51	12.92	-0.035	0.032	0.0785	0.0836	1.999	0.486	0.165
19041	1.84	1.38	0.198	0.393	0.0143	0.0486	2.206	0.400	0.174
19068	8.68	-0.97	-0.801	0.280	0.0051	0.0420	5.776	0.172	0.401
19066	8.97	-0.95	-0.725	0.249	0.0119	0.0467	5.828	0.166	0.401
19029									0.174
19028									0.172
19044	1.75	1.33	0.052	0.139	0.0465	0.0665	2.123	0.430	0.172

REFERENCES

1 Plostins, P., Bornstein, J.A. and White, C.O., "The Transitional Ballistics and Jump Characteristics of a 25 mm Training Projectile with Base Bleed," BRL-TR-2888, U.S. Army Ballistic Research Laboratory, Aberdeen Proving Ground, MD. 21005, March 1988. (AD A224998)

2 Braun, W.F., "The Free Flight Aerodynamics Range," BRL-R-1048, U.S.Army Ballistic Research Laboratory, Aberdeen Proving Ground, MD. 21005, July 1958. (AD 202249)

3 Murphy, C.H., "Free Flight Motion of Symmetric Missiles," BRL-TR-1216, U.S. Army Ballistics Research Laboratory, Aberdeen Proving Ground, MD. 21005, July 1963. (AD 442757)

4 Kent, R.H. and McShane, E.J., "An Elementary Treatment of the Motion of a Spinning Projectile about its Center of Gravity," BRL-R-459, U.S.Army Ballistic Research Laboratory, Aberdeen Proving Ground, MD. 21005, April 1944. (AD 491943)

5 Whyte, R.H. and Houghton, R.C., "Reduction of Range and Yaw Sonde Data Using Numerical Techniques," Contract Report ARBRL-CR-400, U.S. Army Ballistic Research Laboratory, Aberdeen Proving Ground, MD. 21005, May 1979. (AD B039372)

6 Dowdy, D.N., "Exterior Ballistic Flight Characteristics of Projectile 25-mm TPDS-T," Report Number 89-BA-13, U.S. Army Combat Systems Test Activity, Aberdeen Proving Ground, MD. 21005, June 1989.

7 Murphy, C.H., "The Measurement of Non-Linear Forces and Moments by Means of Free Flight Tests," BRL-R-974, U.S. Army Ballistic Research Laboratories, Aberdeen Proving Ground, MD. 21005, February 1956. (AD 93521)

INTENTIONALLY LEFT BLANK.

LIST OF SYMBOLS

a_2	=	cubic lift force coefficient	
C_2	=	cubic overturning moment coefficient	
$\hat{C}_2$	=	cubic Magnus moment coefficient	
C_D	=	$\dfrac{\pm \mid Drag\ Force \mid}{[(1/2)\,\rho V^2 S]}$	
C_{D0}	=	zero-yaw drag coefficient	
$C_{D_{\delta^2}}$	=	quadratic yaw-drag coefficient	
C_{L_α}	=	$\dfrac{\pm \mid Lift\ Force \mid}{[(1/2)\,\rho V^2 S\,\delta]}$	Positive coefficient: Force in plane of total angle of attack, α_t, $\perp$ to trajectory in direction of α_t. (α_t directed from trajectory to missile axis.) $\delta = \sin\alpha_t$.
$C_{L_{\alpha 0}}$	=	zero-yaw lift force coefficient	
C_{l_p}	=	$\dfrac{\pm \mid Roll\ Damping\ Moment \mid}{[(1/2)\,\rho V^2 S\,d\,(pd/V)]}$	Negative coefficient: Moment decreases rotational velocity.
C_{M_α}	=	$\dfrac{\pm \mid Overturning\ Moment \mid}{[(1/2)\,\rho V^2 S\,d\,\delta]}$	Positive coefficient: Moment increases total angle of attack α_t.
$C_{M_{\alpha 0}}$	=	zero-yaw static moment coefficient	
$C_{M_{p\alpha}}$	=	$\dfrac{\pm \mid Magnus\ Moment \mid}{[(1/2)\,\rho V^2 S\,d\,(pd/V)\,\delta]}$	Positive coefficient: Moment rotates nose $\perp$ to plane of α_t in direction of spin.
$C_{M_{p\alpha 0}}$	=	zero-yaw Magnus moment coefficient	

LIST OF SYMBOLS (continued)

For most exterior ballistic uses, where $\dot{\alpha} \approx q$, $\dot{\beta} \approx -r$, the definition of the damping moment sum is equivalent to:

$C_{M_q} + C_{M_{\dot{\alpha}}} \quad = \quad \dfrac{\pm \mid Damping\ Moment \mid}{[(1/2)\rho V^2 S d\,(q_t d/V)]}$ Positive coefficient: Moment increases angular velocity.

$\left(C_{M_q} + C_{M_{\dot{\alpha}}}\right)_0 =$ zero-yaw pitch damping moment coefficient

C_{P_N} = center of pressure of the normal force, positive from base to nose

d = projectile diameter

d_2 = cubic pitch damping moment coefficient

I_x = axial moment of inertia

I_y = transverse moment of inertia

K_F = magnitude of the fast yaw mode

K_S = magnitude of the slow yaw mode

k_x = axial radius of gyration, $k_x^2 = \dfrac{I_x}{md^2}$

k_y = transverse radius of gyration, $k_y^2 = \dfrac{I_y}{md^2}$

l = length of projectile

m = mass of projectile

M = $\left(\dfrac{\rho S d^3}{2 I_y}\right) C_{M_\alpha}$

M_∞ = Mach number

p = roll rate

P = $\dfrac{I_x}{I_y}\,\dfrac{\mathrm{pd}}{\mathrm{V}}$

LIST OF SYMBOLS (continued)

q	=	angular velocity component (about the missile-fixed Y axis)
q_t	=	$(q^2 + r^2)^{\frac{1}{2}}$
r	=	angular velocity component (about the missile-fixed Z axis)
S	=	$(\pi d^2/4)$, reference area
S_d	=	dynamic stability factor
S_g	=	gyroscopic stability factor
V	=	projectile speed
X	=	missile axis of symmetry, positive forward (see Reference (3))
Y	=	cross-plane axis, forming a right handed system (see Reference (3))
Z	=	cross-plane axis, forming a right handed system (see Reference (3))

Greek Symbols

α	=	angle of attack
α_t	=	$(\alpha^2 + \beta^2)^{\frac{1}{2}} = \sin^{-1}\delta$, total angle of attack
β	=	angle of sideslip
δ^2	$\cong$	$\alpha^2 + \beta^2$
$\delta^2_{e_{HH}}$	=	$\left(\frac{I_y}{I_x}\right)\left[\frac{(\phi'_F + \phi'_S)(K_S^2 - K_F^2)}{(\phi'_F - \phi'_S)}\right]$
$\delta^2_{e_{HT}}$	=	$\frac{(\phi'_F K_S^2 - \phi'_S K_F^2)}{(\phi'_F - \phi'_S)}$
$\delta^2_{e_{TH}}$	=	$\left(\frac{I_x}{I_y}\right)\left[\frac{(K_F^2 \phi'^2_F - K_S^2 \phi'^2_S)}{(\phi'^2_F - \phi'^2_S)}\right]$
$\delta^2_{e_{TT}}, \delta^2_e$	=	$K_F^2 + K_S^2 + \frac{(\phi'_F K_F^2 - \phi'_S K_S^2)}{(\phi'_F - \phi'_S)}$

LIST OF SYMBOLS (continued)

Greek Symbols (continued)

λ_F	=	fast mode damping rate	negative λ indicates damping
λ_S	=	slow mode damping rate	negative λ indicates damping
ρ	=	air density	
ϕ'_F	=	fast mode frequency	
ϕ'_S	=	slow mode frequency	

Subscripts

$c.m.$	=	center of mass	
R	=	range value	Example: $[C_D]_R$ is the coefficient value measured in a free-flight spark photography range facility for total drag.

No of Copies	Organization
2	Administrator Defense Technical Info Center ATTN: DTIC-DDA Cameron Station Alexandria, VA 22304-6145
1	HQDA (SARD-TR) WASH DC 20310-0001
1	Commander US Army Materiel Command ATTN: AMCDRA-ST 5001 Eisenhower Avenue Alexandria, VA 22333-0001
1	Commander US Army Laboratory Command ATTN: AMSLC-DL Adelphi, MD 20783-1145
2	Commander US Army, ARDEC ATTN: SMCAR-IMI-I Picatinny Arsenal, NJ 07806-5000
2	Commander US Army, ARDEC ATTN: SMCAR-TDC Picatinny Arsenal, NJ 07806-5000
1	Director Benet Weapons Laboratory US Army, ARDEC ATTN: SMCAR-CCB-TL Watervliet, NY 12189-4050
1	Commander US Army Armament, Munitions and Chemical Command ATTN: SMCAR-ESP-L Rock Island, IL 61299-5000
1	Director US Army Aviation Research and Technology Activity ATTN: SAVRT-R (Library) M/S 219-3 Ames Research Center Moffett Field, CA 94035-1000

No of Copies	Organization
1	Commander US Army Missile Command ATTN: AMSMI-RD-CS-R (DOC) Redstone Arsenal, AL 35898-5010
1	Commander US Army Tank-Automotive Command ATTN: AMSTA-TSL (Technical Library) Warren, MI 48397-5000
1	Director US Army TRADOC Analysis Command ATTN: ATRC-WSR White Sands Missile Range, NM 88002-5502
(Class. only) 1	Commandant US Army Infantry School ATTN: ATSH-CD (Security Mgr.) Fort Benning, GA 31905-5660
(Unclass. only) 1	Commandant US Army Infantry School ATTN: ATSH-CD-CSO-OR Fort Benning, GA 31905-5660
1	Air Force Armament Laboratory ATTN: AFATL/DLODL Eglin AFB, FL 32542-5000
	Aberdeen Proving Ground
2	Dir, USAMSAA ATTN: AMXSY-D AMXSY-MP, H. Cohen
1	Cdr, USATECOM ATTN: AMSTE-TD
3	Cdr, CRDEC, AMCCOM ATTN: SMCCR-RSP-A SMCCR-MU SMCCR-MSI
1	Dir, VLAMO ATTN: AMSLC-VL-D

No. of Copies	Organization
10	Commander US Army, ARDEC ATTN: SMCAR-CCL-CA, P. O'Neill C. A. Miller E. Malatesta G. Fleming Alan Li SMCAR-AEI-A, R. Kline J. Grau Chiu Ng J. Whyte AMSMC-QAF-S, D. Messer Picatinny Arsenal, NJ 07806-5000
3	Commandant US Army Infantry School ATTN: ATSH-CD-MLS-S, SFC Kohlhase ATSH-INA-BPO, SFC Wood ATSH-TD-S-D, V. Hartman Fort Benning, GA 31905-5800
1	Commander HQ, TRAC RPD ATTN: ATCD-MH, CPT J. Williams Fort Monroe, VA 23651-5000
1	Commander US Army Yuma Proving Ground ATTN: STEYP-MT-ET-C, W. Aynes Yuma, AZ 85365-9103
1	Commander Program Manager Bradley Fighting Vehicle System ATTN: AMCPM-BFVS, K. Pitco Warren, MI 48937 5000
1	Commander US Army Armor Center & School ATTN: ATSB-SMT, MAJ Newlin Fort Knox, KY 40121
2	Alliant Techsystems, Inc. ATTN: C. Rippe B. Becker 600 Second Street, NE Hopkins, MN 55343

No. of Copies	Organization
3	Aerojet General Corporation ATTN: E. Daniels J. Parkinson S. Rush P.O. Box 296 Azusa, CA 91702
2	Arrow Tech Associates ATTN: B. Whyte W. Hathaway P.O. Box 4218 South Burlington, VT 05401-0042

Aberdeen Proving Ground

No. of Copies	Organization
4	Dir, USACSTA ATTN: STECS-AA-LA, M. Maule J. Steier M. Feinberg A. Rose
1	Cdr, USATECOM ATTN: AMSTE-TER, B. Marshall
2	Dir, USAMSAA ATTN: AMXSY-GI, D. Hartka CPT Klimack

USER EVALUATION SHEET/CHANGE OF ADDRESS

This Laboratory undertakes a continuing effort to improve the quality of the reports it publishes. Your comments/answers to the items/questions below will aid us in our efforts.

1. BRL Report Number BRL-MR-3886 Date of Report JANUARY 1991

2. Date Report Received ______________________________

3. Does this report satisfy a need? (Comment on purpose, related project, or other area of interest for which the report will be used.) ______________________________

4. Specifically, how is the report being used? (Information source, design data, procedure, source of ideas, etc.) ______________________________

5. Has the information in this report led to any quantitative savings as far as man-hours or dollars saved, operating costs avoided, or efficiencies achieved, etc? If so, please elaborate. ______________________________

6. General Comments. What do you think should be changed to improve future reports? (Indicate changes to organization, technical content, format, etc.) ______________________________

CURRENT ADDRESS

____
Name

____
Organization

____
Address

____
City, State, Zip Code

7. If indicating a Change of Address or Address Correction, please provide the New or Correct Address in Block 6 above and the Old or Incorrect address below.

OLD ADDRESS

____
Name

____
Organization

____
Address

____
City, State, Zip Code

(Remove this sheet, fold as indicated, staple or tape closed, and mail.)

---FOLD HERE---

DEPARTMENT OF THE ARMY

Director
U.S. Army Ballistic Research Laboratory
ATTN: SLCBR-DD-T
Aberdeen Proving Ground, MD 210[illegible]-5066
OFFICIAL BUSINESS

NO POSTAGE
NECESSARY
IF MAILED
IN THE
UNITED STATES

BUSINESS REPLY MAIL
FIRST CLASS PERMIT No 0001, APG, MD

POSTAGE WILL BE PAID BY ADDRESSEE

Director
U.S. Army Ballistic Research Laboratory
ATTN: SLCBR-DD-T
Aberdeen Proving Ground, MD 21005-9989

---FOLD HERE---